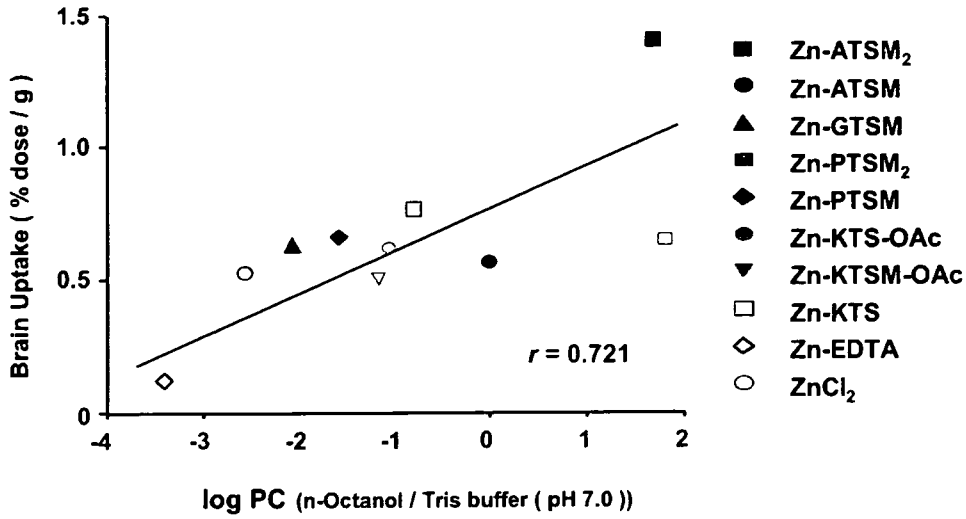

Fig. 9 Relationship between uptake in the brain and the octanol : Tris buffer (pH 7.0) partition coefficient (log P) for [65] Zn-BTS complexes.
Uptake was expressed as % dose/ g of tissue at 1 h post-injection of radiolabeled compounds into mice.

membranes and provide protection against NMDA receptor-mediated glutamate neurotoxicity, would seem to be a therapeutic drug for the prevention of ischemic neuronal damage.

Our previous studies demonstrated that bis(thiosemicarbazone) (BTS) derivatives formed stable chelates with divalent cations like copper and zinc ions, and that certain BTS complexes of Cu^{2+} were readily distributed in cerebral tissues because of greater membrane permeability [30-34]. Thus, we synthesized several Zn-BTS chelates and assessed their biodistribution, especially their uptake into the brain. It was found that the uptake basically increased along with the lipophilicity of the compound and, among the zinc complexes tested, the 2,3 -butanedione bis(N-dimethylthiosemicarbazonato) zinc complex (Zn-$ATSM_2$) displayed the highest cerebral level, 2.7-fold that of Zn^{2+} at 1 h post-injection (Fig. 9) [31]. No adverse effect on behavior was observed after the administration of these zinc compounds [35].

The protective effect of Zn-$ATSM_2$ on the neurotoxicity of glutamate was examined in cultured retinal neurons and compared with that of Zn^{2+} because the retina is rich in glutamatergic neurons [36]. Glutamate treatment markedly reduced cell viability and the addition of Zn^{2+} markedly reversed this tendency. Zn-$ATSM_2$ provided protection against this neurotoxicity and the effect was similar to that of Zn^{2+}, whereas the ligand, $ATSM_2$, did not affect cell viability (Fig 10) [37].

Furthermore, we examined the effects in vivo of systemically administered Zn-$ATSM_2$ on ischemic neuronal injury using the rodent model. Compared with the control group, the infarct volume in the Zn-$ATSM_2$-treated groups 30min before the onset of occlusion and immediately after reperfusion, was significantly reduced. Furthermore, no morphological or physiological alterations were observed after the injection of Zn-$ATSM_2$. Thus, Zn

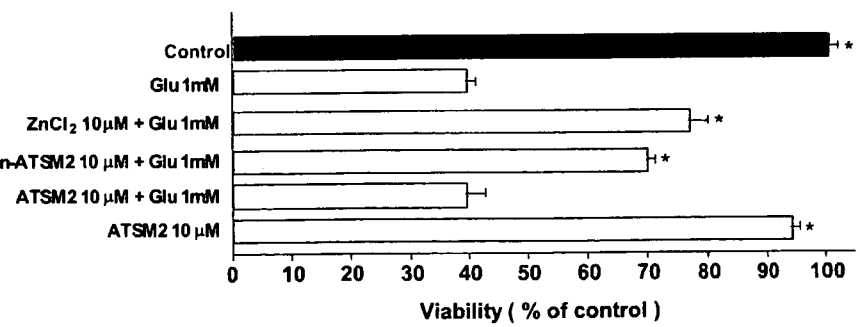

Fig. 10 The effects of Zn-$ATSM_2$, Zn^{2+} on glutamate-induced retinal neurotoxicity.
Neurotoxicity was induced by 1 mM glutamate (Glu). *P < 0.05 vs. Group treated with glutamate (Student's t-test). Values are the mean ± SEM. (n = 5).

-$ATSM_2$ with good ability to permeate the blood-brain barrier, had protective effects on the brain when systemically administered early in a model of temporary focal ischemia.

References

1) Saji H : Targeted Delivery of Radiolabeled Imaging and Therapeutic Agents : Bifunctional Radiopharmaceuticals. Critical Reviews in Therapeutic Drug Carrier Systems. 16 : 209-244, 1999.
2) Verbruggen AM : Bifunctional chelators for technetium-99m. Mather SJ (ed) : Current Directions in Radiopharmaceutical Research and Development. Kluwer Academic Publishers, Dordrecht, 1996, pp 31-46..
3) Dilworth JR and Parrott SJ : Radiopharmaceutically relevant chemistry of technetium and rhenium. Mather SJ (ed) : Current Directions in Radiopharmaceutical Research and Development. Kluwer Academic Publishers, Dordrecht, 1996, pp 1-29.
4) Holman BL, Hellman RS, Goldsmith SJ, Mena IG., Leveille J, Gerundidi Gherrardi P, Moretti JL, Bischof-Delaloye A, Hill TC and Rigo PM : Biodistribution, dosimetry, and clinical evaluation of technetium-99m ethyl cysteinate dimer in normal subjects and in patients with chronic cerebral infarction. J Nucl Med, 30 : 1018-1024, 1989.
5) Walovitch RC, Hill TC, Garrity ST, Cheesman EH, Burgess BA, OLeary DH, Watson AD, Ganey MV, Morgan RA and Williams SJ : Characterization of technetium-99m-L,L-ECD for brain perfusion imaging, Part 1 : pharmacology of techetium-99m ECD in nonhuman primates. J Nucl Med, 30 : 1892-1901, 1989.
6) Leveille J, Demonceau G., De Roo M, Rigo P, Tailefer R, Morgan RA, Kupranick D and Walovitch RC : Characterization of technetium-99 m-L,L-ECD for brain perfusion imaging, Part 2 : biodistribution and brain imaging in humans, J Nucl Med, 30 : 1902-1910, 1989.
7) Horiuchi KS and Yokoyama A : Radioactive metal complexes used for tumor diagnosis. Berthon G. (ed) : Handbook of Metal-Ligand Interactions in Biological Fluids. Mercel Dekker, New York, 1995, pp 1052-1066.
8) Jurisson S, Berning D, Jia W and Ma D : Coordination compounds in nuclear medicine. Chem Rev, 93 : 1137-1156, 1993.
9) Fischman AJ, Badich JW and Strauss HW : A ticket to ride ; peptide radiopharmaceuticals. J Nucl Med, 34 : 2253-2263, 1993.
10) Hom RK, and Katzenellenbogen JA : Technetium-99m-labeled receptor-specific small-molecule radiopharmaceuticals : recent developments and encouraging results. Nucl Med Biol, 24 : 485-498, 1997.
11) Portenoy RK, Lesage P : Management of cancer pain. Lancet. 353 : 1695-1700, 1999.
12) Lewington VJ : Bone-seeking radionuclides for therapy. J Nucl Med 46 : Suppl 1 : 38S-47S, 2005.
13) Lam MG, de Klerk JM, van Rijk PP : ^{186}Re-HEDP for metastatic bone pain in breast cancer patients. Eur J Nucl Med Mol Imaging 31 : Suppl 1 : S162-170, 2004.
14) de Klerk JM, van Dijk A, van het Schip AD, Zonnenberg BA, van Rijk PP : Pharmacokinetics of rhenium-186 after administration of rhenium-186-HEDP to patients with bone metastases. J Nucl Med 33 : 646-651, 1992.
15) de Winter F, Brans B, Van De Wiele C, Dierckx RA. : Visualization of the stomach on rhenium-186 HEDP imaging after therapy for metastasized prostate carcinoma. Clin Nucl Med. 24 : 898-899, 1999.
16) Ogawa K, Mukai T, Arano Y, Hanaoka H, Hashimoto K, Nishimura H, and Saji H. : Design of a radiopharmaceutical for the palliation of painful bone metastases : rhenium-186-labeled bisphosphonate derivative. J Labelled Cmp Radiopharm 47 : 753-761, 2004.
17) Fleisch H : Bisphosphonates : mechanisms of action.. Endocr Rev 19 : 80-100, 1998.
18) van Beek E, Hoekstra M, van de Ruit M, Lowik C, Papapoulos S : Structural requirements for bisphosphonate actions in vitro. J Bone Miner Res 9 : 1875-1882, 1994.
19) Ogawa K, Mukai T, Arano Y, Otka A, Ueda M, Uehara T, Magata Y, Hashimoto K and Saji H : Rhemium-186-monoaminemonoamidedithiols conjugated bisphosphonate derivatives for bone pain palliation. Nucl Med Biol 33 : 513-520, 2006.
20) Ogawa K, Mukai T, Arano Y, Ono M, Hanaoka H, Ishino S, Hashimoto H, Nishimura H and Saji H : Development of a rhenium-186-labeled MAG3-conjugated bisphosphonate for the palliation of metastatic bone pain based on the concept of bifunctional radiopharmaceuticals. Bioconjug Chem 16 : 751-757, 2005.
21) Frederickson CJ : Neurobiology of zinc and zinc-containing neurons. Int Rev Neurobiol 31 : 145-238,

1989.

22) Ueno S, Tsukamoto M, Hirano T, Kikuchi K, Yamada MK, Nishiyama N, Nagano T, Matsuki N and Ikegaya Y : Mossy fiber Zn^{2+} spillover modulates heterosynaptic N-methyl-D-aspartate receptor activity in hippocampal CA3 circuits. J Cell Biol **158** : 215-220, Epub 2002 Jul 2015, 2002.

23) Howell GA, Welch MG. and Frederickson CJ : Stimulation-induced uptake and release of zinc in hippocampal slices. Nature **308** : 736-738, 1984.

24) Smart TG, Xie X and Krishek BJ : Modulation of inhibitory and excitatory amino acid receptor ion channels by zinc. Prog Neurobiol **42** : 393-341, 1994.

25) Koh JY, Suh SW, Gwag BJ, He YY, Hsu CY and Choi DW : The role of zinc in selective neuronal death after transient global cerebral ischemia. Science **272** : 1013-1016, 1996.

26) Kitamura Y, Iida Y, Abe J, Ueda M, Mifune M, Kasuya F, Ohta M, Igarashi K, Saito Y and Saji H : Protective effect of zinc against ischemic neuronal injury in a middle cerebral artery occlusion model. J Pharmacol Sci **100** : 142-148, 2006.

27) Kitamura Y, Iida Y, Abe J, Mifune M, Kasuya F, Ohta M, Igarashi K, Saito Y and Saji H : In vivo measurement of presynaptic Zn2+ release during forebrain ischemia in rats. Biol Pharm Bull **29** : 821-823, 2006.

28) Kitamura Y, Iida Y, Abe J, Mifune M, Kasuya F, Ohta M, Igarashi K, Saito Y and Saji H : Release of vesicular Zn(2+) in a rat transient middle cerebral artery occlusion model. Brain Res Bull **69** : 622-625, 2006.

29) Peynolds IJ and Miller RJ : [^{3}H]MK801 binding to the NMDA receptor / ionophore complex is regulated by divalent cations : evidence for multiple regulatory sites. Eur J Pharmacol 151 : 103-112, 1988.

30) Gingras BA, Suprunchuk T and Bayley CH : The preparation of some thiosemicarbazones and their copper complexes. Can J Chem 40 : 1053-1059, 1962.

31) Green MA, Kippenstein DL and Tennison JR : Copper(II) bis(thiosemicarbazone) complexes as potential tracers for evaluation of cerebral and myocardial blood flow with PET. J Nucl Med 29 : 1549-1557, 1988.

32) John EK and Green MA : Structure-activity relationships for metal-labeled blood flow tracers : comparison of keto aldehyde bis(thisemocarbazonato)copper(II) derivatives. J Med Chem 33 : 1764-1770, 1990.

33) Saji H, Saiga A, Iida Y, Magata Y and Yokoyama A : Synthesis and in vivo behavior of a copper-64-labeled dithiosemicarbazone derivative coupled to a dihydropyridine carrier. J Label Comp Radiopharm 33 : 127-135, 1993.

34) Wada K, Fujibayashi Y and Yokoyama A : Copper (II) [2,3-butanedionebis (N^4-methylthiosemicarbazone)], a stable superoxide dismutase-like copper complex with high membrane penetrability. Arch Biochem Biophys 310 : 1-5, 1994.

35) Saji H, Kinoshita T, Kubota M, Kaneda K, Akaike A, Kikuchi M, Kashii S, Honda Y, Iida Y, Magata Y, Yokoyama A. Brain permeable zinc complex with neuroprotective action. s.t.p. Pharma Sci 7 : 92 -97, 1997.

36) Karcioglu ZA : Zinc in the eye. Surv Ophthalmol 27 : 114-122, 1982.

37) Kubota M, Iida Y, Magata Y, Kitamura Y, Kawashima H, Saji H : Mechanisom of [2,3-butanedione bis(N^4-dimethylthiosemicarbazone)zinc (Zn-ATSM2)-induced protection of cultured hippocampal neurons against N-methyl-d-asparatate receptor-mediated glutamate cytotoxicity. Jan J Pharmaco 84 : 334-338, 2000.

Temporal Change in Human Nicotinic Acetylcholine Receptor After Smoking Cessation: 5IA SPECT Study

Marcelo Mamede[1], Koichi Ishizu[1], Masashi Ueda[2], Takahiro Mukai[1], Yasuhiko Iida[2], Hidekazu Kawashima[2], Hidenao Fukuyama[3], Kaori Togashi[1], and Hideo Saji[2]

[1]Department of Diagnostic Imaging and Nuclear Medicine, Graduate School of Medicine, Kyoto University, Kyoto, Japan; [2]Department of Patho-Functional Bioanalysis, Graduate School of Pharmaceutical Science, Kyoto University, Kyoto, Japan; and [3]Brain Function Imaging Division, Human Brain Research Center, Graduate School of Medicine, Kyoto University, Kyoto, Japan

Nicotinic acetylcholine receptors (nAChRs) are of great interest because they are implicated in various brain functions. They also are thought to play an important role in nicotine addiction of smokers. Chronic (−)-nicotine, a nAChR agonist, treatment in mice and rats elicits a dose-dependent increase in nAChRs in the brain. Upregulation of nAChRs in postmortem human brains of smokers has also been reported. However, changes in nAChRs after cigarette smoking cessation in humans are poorly understood. The aim of this study was to detect the dynamic changes of nAChRs after smoking and smoking cessation in the brains of living subjects. **Methods:** We performed 5-^{123}I-iodo-A-85380 (^{123}I-5IA) SPECT on nonsmokers and smokers (n = 16) who had quit smoking for 4 h, 10 d, and 21 d and calculated and compared distribution volumes (Vt) of ^{123}I-5IA. **Results:** The binding potential of nAChRs (Vt of ^{123}I-5IA) in the brains of smokers decreased by 33.5% ± 10.5% after 4 h of smoking cessation, increased by 25.7% ± 9.2% after 10 d of smoking cessation, and decreased to the level of nonsmokers after 21 d of smoking cessation. **Conclusion:** Because the upregulation of the nAChRs of the smokers after chronic exposure of the nicotine was downregulated to the nonsmokers' level by around 21 d after smoking cessation, the upregulation is a temporary effect. The decrease in nicotinic receptors to nonsmoker levels may be the breaking point during the nicotine withdrawal period.

Key Words: ^{123}I-5IA; SPECT; nicotinic acetylcholine receptors; human brain; smoking withdrawal; quantitative measurement

J Nucl Med 2007; 48:1829–1835
DOI: 10.2967/jnumed.107.043471

Nicotinic acetylcholine receptors (nAChRs) are a family of ligand-gated ion channels that regulate neurotransmission in the central and peripheral nervous systems. These receptors are of great interest because they are implicated in various brain functions, including cognition and memory (*1,2*) and in nicotine-induced neuroprotective (*3*) and analgesic effects (*4*). In addition, these receptors are thought to play an important role in nicotine addiction (*5*).

Chronic treatment with agonists for most neurotransmitter receptor systems results in a decrease in receptor number. However, it has been demonstrated that chronic treatment of mice (*6*) and rats (*7*) with (−)-nicotine, an nAChR agonist, elicits a dose-dependent increase in nAChRs. This upregulation is not permanent, returning to control levels within 7–10 d in mice (*6*) and 15–20 d in rats (*8,9*) after cessation of (−)-nicotine treatment. Previous efforts to demonstrate nAChR upregulation in the human brain have also been reported primarily in in vitro binding assays (*10,11*). Kassiou et al. reported the upregulation of nAChRs with chronic (−)-nicotine treatment in the brain of a live baboon (*12*). More recently, Staley et al. described the upregulation of nAChRs in human brains after early abstinence of tobacco smoking using 5-^{123}I-iodo-A-85380 (^{123}I-5IA) and SPECT images (*13*). However, changes in nAChRs in humans after cessation of smoking are poorly understood. Breese et al. studied the levels of ^{3}H-nicotine binding in humans postmortem for changes in nicotinic receptor levels and reported that the nAChR levels in smokers who had stopped smoking at least 2 mo before their death were similar to those in nonsmokers (*14*); the effects of shorter-term smoking cessation are unknown.

^{123}I-5IA is a nAChR imaging probe that has extremely high selectivity and specificity for the α4β2 subunit of nAChRs in rodent (inhibition constant = 0.37 nM) (*15*) and primate brain in vivo (*16*), with relatively low acute toxicity (effective dose equivalent = 30 μSv/MBq) (*17,18*). Moreover, we have developed the methodology for the quantification of nAChRs in human brain using ^{123}I-5IA and SPECT (*19*).

The aim of the present study was to detect the dynamic changes of nAChRs in living human brain after smoking and smoking cessation. We performed ^{123}I-5IA SPECT on nonsmokers and smokers who had quit smoking for 4 h, 10 d, and

Received May 9, 2007; revision accepted Jul. 30, 2007.
For correspondence or reprints contact: Koichi Ishizu, MD, PhD, Department of Diagnostic Imaging and Nuclear Medicine, Graduate School of Medicine, Kyoto University, Sakyo, 606-8507, Kyoto, Japan.
E-mail: ishizu@kuhp.kyoto-u.ac.jp

21 d and compared the distribution volumes (*Vt*) of ^{123}I-5IA of each group and with nonsmokers. To our knowledge, this is the first in vivo imaging study of nAChR upregulation and recovery in response to short-term smoking cessation in living subjects.

MATERIALS AND METHODS

Volunteers

Six male nonsmokers (23 ± 6 y) and 10 healthy male smokers (28 ± 4 y) were included in this study. Five smokers in the 4-h group were also included in either the 10-d or the 21-d group. In total, 21 ^{123}I-5IA SPECT studies were acquired (Table 1). None of the subjects had a history of neurologic or psychiatric illness or the use of psychotropic or sleep-inducing drugs. The nonsmokers had no history of smoking tobacco.

For the smoking withdrawal studies, the smokers were divided in 3 groups: 5 subjects (age, 28 ± 4 y) for 4-h withdrawal, 5 subjects (age, 27 ± 6 y) for 10-d withdrawal, and 5 subjects (age, 28 ± 3 y) for 21 d of smoking withdrawal. The 4 groups were age-matched.

All subjects gave written informed consent to participate in this study in compliance with the regulations of the Joint Committee on Clinical Investigation of the Kyoto University Hospital.

Radiolabeling

Radiolabeling of the ^{123}I-5IA followed the methods we reported previously (*19*). To a sodium ^{123}I-iodide solution (1,110 MBq) (Nihon Medi-Physics), 100 μg of (*S*)-5-(tri-*n*-butylstannyl)-3-([1-*t*-butoxycarbonyl-2(*S*)-azetidinyl]methoxy)pyridine, 1.5% acetic acid, 3 mol/L HCl, and 5% H_2O_2 solution were added, and the mixture was stirred at 75°C for 15 min. Concentrated HCl was then added, and the resulting solution was stirred for another 10 min at 75°C. The mixture was made basic with NaOH and extracted with ethyl acetate, and the organic layer was evaporated. The residue was purified by reverse-phase high-performance liquid chromatography ([HPLC] Cosmosil 5C18-AR-300, 10 × 250 mm; Nacalai Tesque; 10 mmol/L ammonium acetate/methanol/triethylamine = 752:750:2; 1.5 mL/min; retention time for 5IA was 40 min). After evaporation of the HPLC eluent, the residue was dissolved in 0.9% saline and filtered through a 0.2-μm filter into a sterile vial. Radiochemical purity was >98%, and radiochemical yields were ~42%. The specific activity determined from the ultraviolet absorbance at 254 nm was >169 GBq/μmol (the detection limit for this method).

SPECT

All subjects underwent a set of 5 SPECT dynamic scans (a 120-min scan, followed by 4 sets of 20-min scans). All SPECT dynamic scans were acquired with a triple-head rotating γ-camera system (PRISM 3000; Picker International) equipped with low-energy, high-resolution, fanbeam collimators. Data acquisition and image reconstruction were performed as in our previous study (*19*). The data acquisition was alternately performed over 120 min after intravenous injection of ^{123}I-5IA, followed by 4 sets of 20-min scans (at 3, 4, 5, and 6 h after the injection). SPECT images were reconstructed using a filtered backprojection algorithm with a ramp filter. Attenuation correction was performed using ellipses outer line approximation and Chang's method (coefficient of 0.06/cm), which assumes that the attenuation process is homogeneous throughout the brain and can be described by an exponential function. Scatter correction was not applied.

A dose of ~150 MBq of ^{123}I-5IA was administered intravenously over a period of 1 min at a constant rate with an infusion pump, and the SPECT scan was started at the same time as the injection. Arterial blood sampling and metabolite correction were also performed to estimate the arterial input function of the ^{123}I-5IA for each volunteer by the same method as that used in our earlier study (*19*).

TABLE 1
Study Groups

Nonsmokers	Smokers: period of smoking cessation		
	4 h	10 d	21 d
Subject 1	Subject 7	Subject 7	Subject 9
Subject 2	Subject 8	Subject 8	Subject 10
Subject 3	Subject 9	Subject 12	Subject 11
Subject 4	Subject 10	Subject 13	Subject 15
Subject 5	Subject 11	Subject 14	Subject 16
Subject 6			

Arterial Input Function

Twenty-five arterial blood samples were obtained at the same time points as described previously (*19*). From each sample, 100 μL of plasma were removed and the radioactivity was measured in an automatic well-type γ-counter (Cobra 2; Packard Instruments). Sixteen samples were analyzed by thin-layer chromatography (TLC) (10% ammonium acetate and methanol [1:1], LK6DF Silica Gel, 60 Å; Whatman) for metabolite determination (R_f = 0.55 for ^{123}I-5IA) (*19*). The measured unmetabolized fractions were fitted with a dual exponential curve, and the input function was calculated as all plasma sample counts were corrected for metabolites using the fitted curve.

Data Analysis

Reconstructed SPECT images were automatically coregistered using a coregistration algorism of statistical parametric mapping, SPM99 (Welcome Department of Cognitive Neurology, London, U.K.), to minimize positional error caused by head movement during the scans. Multiple circular regions of interest (ROIs) (21 pixels per circle) were manually drawn in each brain region (basal ganglia, thalamus, brain stem, cerebellum, frontal, parietal, temporal, and occipital cortices) on both sides. ROI data were further decay-corrected. SPECT data were calibrated to the well counter used to measure the injected activity. Time–activity curves were generated from the ROIs and the dynamic image datasets.

Kinetic analysis of the ^{123}I-5IA was performed using a 2-compartment model including K_1 and k_2 rate constants and a curve-fitting method following our previous study (*19*). *Vt* values of the ^{123}I-5IA were calculated and used as a quantitative index correlated with the regional binding potential of the nAChRs. The *Vt* values were further evaluated in terms of interval change after the smoking withdrawal.

Statistical Analysis

All data are expressed as the mean ± SD. The *Vt* values obtained from the different regions in the brain were analyzed by 1-way ANOVA with the Bonferroni protected least significant difference test. The interval changes of the ^{123}I-5IA *Vt* were analyzed between the 3 phases after the smoking withdrawal using the Tukey–Kramer multiple comparison test. All tests were 2-sided, and probability values of $P < 0.05$ were considered significant.

RESULTS

As in our previous study (*19*), the characteristics of the arterial input functions for all volunteers (nonsmokers and smokers) were similar. The peak plasma activity occurred between 70 and 80 s after injection in all subjects and decreased rapidly to 6.5%−9.0% of the peak level in 10 min. Analysis of the unmetabolized compound by TLC demonstrated a high parent fraction of ^{123}I-5IA in the plasma (87.7% ± 6.3%) in the first minute. ^{123}I-5IA was rapidly metabolized, and the unchanged fraction represented 50.9% ± 8.8% and 32.4% ± 12.6% of total plasma activity at 20 and 60 min, respectively.

Figure 1 shows the representative standardized time–activity curve of ^{123}I-5IA in the frontal cortex. The concentrations of radioactivity were slightly higher in the nonsmokers and in the 4-h smoking-cessation group followed by the 10-d and 21-d smoking-cessation groups. The peaks of radioactivity occurred ~50 min after injection of ^{123}I-5IA for nonsmokers and for the 4-h and 21-d smoking-cessation groups, whereas it was at ~70 min for the 10-d smoking-cessation group. A differential dissociation of ^{123}I-5IA from the binding sites was noted in the brain. The 4-h smoking-cessation group showed a faster dissociation compared with that of the nonsmokers. However, the 10-d and 21-d smoking-cessation groups showed a slower dissociation than that of the nonsmokers (more pronounced in the 21-d group). These findings reflected a temporal change of the nAChRs in the human brain.

Packs per day and pack years of cigarette smoking before cessation were similar for the different groups of smokers (Table 2). Only 2 subjects (subjects 7 and 11) had detectable amounts of nicotine in their plasma after 4-h smoking cessation (Table 2).

To validate the *Vt* values of the nonsmokers as a baseline group, we compared (*t* test) our current data (nonsmokers) with our published data (*19*). No significant difference was observed between these groups. Similar findings were also seen for K_1 and k_2. Therefore, we used the *Vt* values from nonsmokers as a reference for further comparisons with groups of smokers at several smoking-cessation intervals.

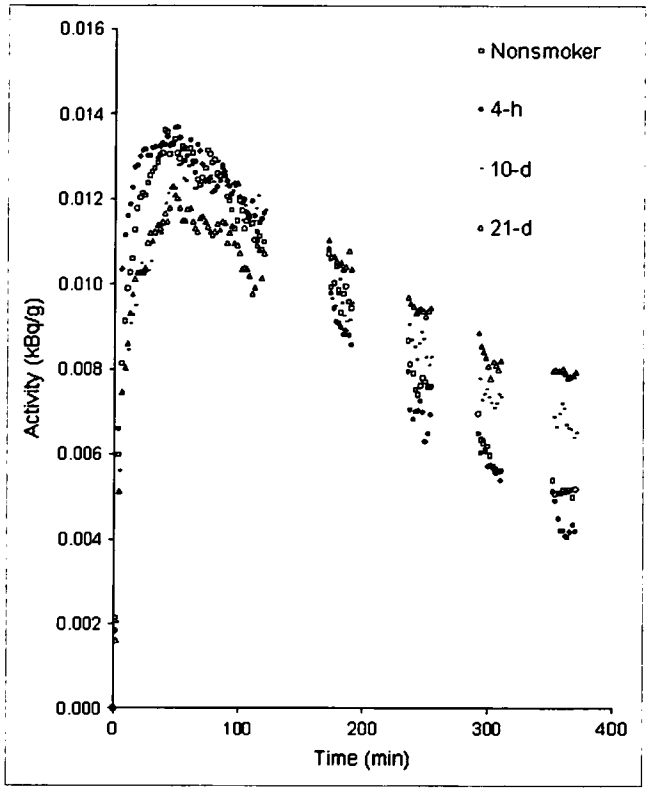

FIGURE 1. Representative standardized time–activity curves of ^{123}I-5IA in frontal cortex from a nonsmoker and smokers.

Table 3 describes the *Vt* values of different groups of volunteers (nonsmokers and smokers). There was a significant difference among those groups (ANOVA; $P < 0.001$). Individualized comparisons between 2 groups of volunteers were also performed. After 4 h of smoking cessation, the *Vt* values in all brain regions decreased significantly compared with those of the nonsmoker group ($P < 0.05$, except for frontal, parietal, and occipital cortices). On the other hand, after 10 d of smoking cessation, the *Vt* values were significantly higher than those of nonsmokers ($P < 0.05$, except for basal ganglia and thalamus). Then, after 21 d of smoking cessation, the *Vt* values decreased significantly compared

TABLE 2
Characteristics of Volunteers and Plasma Concentration of Nicotine and Cotinine

Group	Age (y ± SD)	Packs/d	Pack years	Plasma concentration (ng/mL)	
				Nicotine	Cotinine
Nonsmokers	24 ± 6	—	—	ND	ND
Smokers					
4-h withdrawal	28 ± 4	0.8 ± 0.3	6.1 ± 4.3	7.6, 8.9*	282 ± 189
10-d withdrawal	27 ± 6	0.8 ± 0.2	6.3 ± 3.9	ND	ND
21-d withdrawal	28 ± 3	0.8 ± 0.3	6.3 ± 4.5	ND	ND

*Results from only 2 subjects (3 other subjects had nondetectable values).

Packs/d = number of packs smoked per day; Pack years = number of packs per day while smoking multiplied by number of years smoked; ND = not detected (detection limits for nicotine and cotinine were 5.0 and 100 ng/mL, respectively).

Values are expressed in mean ± SD.

TABLE 3

^{123}I-5IA V_t Estimates for 2-Compartment, 2-Parameter Model for Various Brain Regions from Nonsmokers and Smokers After Withdrawal of Cigarette Smoking

Subject	Frontal	Parietal	Temporal	Occipital	BG	Thalamus	BS	Cerebellum
Nonsmokers								
1	14.3	13.2	13.2	11.2	15.8	30.1	22.9	15.6
2	20.3	18.9	19.7	16.2	24.2	43.2	35.5	20.5
3	14.1	13.0	13.8	11.2	16.0	28.4	22.3	14.9
4	14.4	14.4	14.6	11.7	17.2	31.1	25.3	18.4
5	11.3	10.7	10.7	9.5	12.9	19.3	17.7	14.4
6	13.2	12.2	12.2	11.1	13.5	20.9	18.7	13.7
Mean	14.6	13.7	14.0	11.8	16.6	28.8	23.7	16.3
SD	3.0	2.8	3.1	2.3	4.0	8.6	6.4	2.7
Smokers								
4-h withdrawal								
7	6.1	6.3	6.4	5.9	6.5	7.0	7.0	5.9
8	12.6	13.0	12.2	11.4	12.8	16.1	14.0	11.3
9	14.9	14.0	13.7	12.5	15.0	21.3	19.4	14.4
10	8.7	8.4	8.6	7.6	10.0	13.5	12.2	8.8
11	10.2	10.4	10.2	9.0	11.2	12.9	12.3	10.0
Mean	10.5	10.4	10.2	9.3	11.1	14.1	13.0	10.1
SD	3.4	3.2	2.9	2.7	3.2	5.2	4.4	3.1
10-d withdrawal								
7	19.7	19.3	19.2	17.5	21.0	31.1	29.4	20.9
8	19.1	18.7	17.4	16.4	19.4	28.7	25.3	20.7
12	18.0	17.6	17.4	16.1	20.2	28.9	30.3	22.4
13	16.1	16.2	16.4	15.2	18.7	28.9	29.3	20.8
14	19.2	18.1	17.8	15.8	21.5	36.5	32.8	23.9
Mean	18.4	18.0	17.6	16.2	20.2	30.8	29.4	21.7
SD	1.4	1.2	1.0	0.9	1.2	3.3	2.7	1.4
21-d withdrawal								
9	15.3	14.6	14.6	12.2	17.6	28.4	23.6	19.7
10	14.4	14.3	13.8	12.1	17.5	31.3	24.9	17.2
11	17.0	16.6	15.9	13.6	18.5	27.0	26.1	20.1
14	14.1	14.0	13.6	12.8	15.5	21.6	21.0	15.7
15	14.4	14.1	13.6	12.2	15.7	27.0	22.7	15.7
Mean	15.1	14.7	14.3	12.6	17.0	27.0	23.7	17.7
SD	1.2	1.1	1.0	0.6	1.3	3.5	2.0	2.1

BG = basal ganglia; BS = brain stem.
Reported as mean for V_t estimates from 2-compartment model. Values for V_t are in mL/g.

with those of the 10-d group ($P < 0.01$, except for thalamus), returning to the level in nonsmokers (*Vt* values did not show any significant difference compared with those in the nonsmokers). Figure 2 shows the percentage of reduction and increment in each group of smokers in comparison with the nonsmoker group. In the Tukey–Kramer multiple comparison test, the interval changes of the ^{123}I-5IA *Vt* between the 3 phases after the smoking cessation were significantly different ($P < 0.001$).

The rate constant K_1 had some fluctuations among the different groups of volunteers (nonsmokers and smokers); however, these differences were not statistically significant (ANOVA; not significant) (Fig. 3A). On the other hand, the values of the rate constant k_2 were significantly different among the groups of volunteers (ANOVA; $P < 0.01$) (Fig. 3B). This difference was due basically to the increase of k_2 in the group with 4 h of smoking cessation.

DISCUSSION

The present study described the effect of nicotine intake in tobacco smokers and smoking cessation on the high-affinity nicotinic receptors in humans using ^{123}I-5IA SPECT. To our knowledge, this is the first in vivo imaging of nAChR up-regulation and recovery in response to short-term smoking cessation in living smokers.

Previous animal studies have shown that chronic nicotine treatment induces an increase in high-affinity nicotinic receptor binding (*6–9*), and human postmortem studies have found a similar increase in ^{3}H-nicotine binding to high-affinity receptors in the postmortem cortex, cerebellum, and hippocampus of smokers compared with that in nonsmokers (*10–12*).

The mechanism by which the chronic exposure of nicotine evokes an increase in the density of the binding sites is not fully understood. Marks et al. reported that the increase in nicotinic receptor numbers in rodents is not caused by an

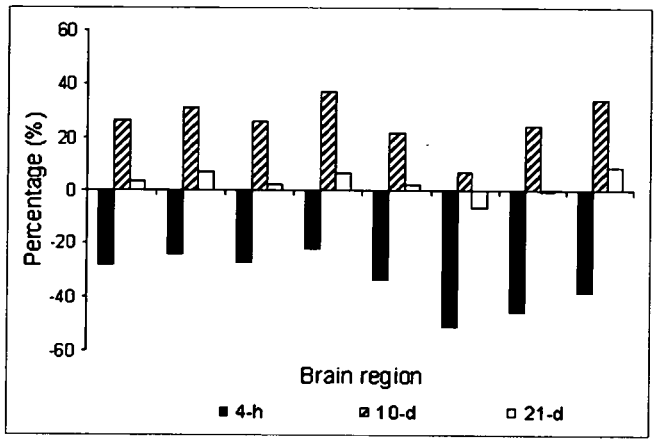

FIGURE 2. Percentage of reduction and increment of *Vt* of ^{123}I-5IA in smokers after smoking cessation compared with nonsmokers. Eight brain regions are frontal, parietal, temporal, occipital, basal ganglia, thalamus, brain stem, and cerebellum from the left, respectively.

increase in messenger RNA levels (*20*). The lack of an effect on nicotinic receptor transcription in mice suggests that nicotine-induced increases in nicotinic receptor levels are most likely related to a decrease in receptor turnover (*21*). The increase in nicotinic receptor number and the decreased rate of receptor turnover may be related to nicotinic receptor channel desensitization, which appears to reflect the conformational state of the receptor channel (*21,22*). Once the nicotinic receptor channels are desensitized and rendered inactive, additional receptors would be recruited to maintain the nicotinic response of the neuron, which results in an overall increase in nicotine binding, possibly due to a conversion of low-affinity receptors to a conformation with a high affinity for agonists (*23*).

In this study, the ^{123}I-5IA *Vt* measured at 4 h after smoking cessation was significantly lower than that in nonsmokers. The mean value of the calculated *Vt* of the smokers was ~33.5% ± 10.5% lower than that of nonsmokers and was more pronounced in the thalamus (51%) and brain stem (45%). In this group of volunteers, the plasma nicotine level 4 h after smoking cessation was detectable in only 2 subjects and was below the detection limit in the other subjects. Nicotine is highly lipophilic and demonstrated high levels of nonspecific uptake in brain (*24,25*). Rowell and Li have reported that levels of nicotine in the brain were ~3-fold higher than those in the plasma (*7*), which explains the lack of plasma nicotine measurements in 3 subjects in this group of volunteers. Because of high levels of nonspecific uptake of nicotine in the brain, nicotine or its metabolites may accumulate in nonspecific compartments in the brain (i.e., white matter) and then diffuse slowly into areas with higher levels of nAChRs, maintaining high levels of occupancy of the nAChRs. In addition, Brody et al. have shown saturation of the nicotinic receptors in human brain for up to 4 h in smokers (*26*). Thus, we would expect some level of nicotine or metabolites in the brain that would compete with ^{123}I-5IA and impair imaging of the upregulation of nAChRs. Also, we believe that some level of nicotine in the brain resulted in a high level of occupancy of the receptors, which reduced specific tracer uptake (*27*). Because of competitive binding between the radioligand and nicotine in the brain, imaging of upregulation of nAChRs in vivo requires sufficient time for nicotine clearance (>4-h smoking cessation).

After 10 d of smoking cessation, the *Vt* of ^{123}I-5IA was significantly higher than that in nonsmokers, with a 25.7% ± 9.2% increase among brain regions. The result of the increased *Vt* of the ^{123}I-5IA was in agreement with the upregulation of the nAChRs in the brains of smokers reported in postmortem human studies (*10–12*) and in animal studies (*6–9*). Staley et al. have described similar findings in human brain (*13*). The authors noted that after 6.8 ± 1.9 d of tobacco abstinence, the uptake of ^{123}I-5IA increased significantly throughout the cerebral cortex (26%~36%) in smokers (*13*). After 10 d of smoking cessation, nicotine and cotinine were not detected in the plasma. Thus, blood nicotine levels were negligible in the ^{123}I-5IA SPECT scans of smokers as well as nonsmokers.

After 21 d of smoking cessation, the *Vt* of ^{123}I-5IA was significantly lower compared with that after 10 d of smoking cessation and was not significantly different from that in the nonsmokers. Breese et al. showed that smokers who had quit at least 2 mo before death had nicotinic receptor binding levels similar to those in nonsmokers (*14*). In the present study, the interval of 21 d was thought to be the recovery time during which upregulated nAChRs return to the level of the nonsmoker. This suggests that nicotine-induced upregulation of receptor number is a temporary effect, similar to that found in rodents (*28,29*).

The upregulation of the nAChRs was similar in almost all brain regions, except the thalamus and basal ganglia, which showed a slightly different pattern. In thalamus and basal ganglia, after 10 d of smoking cessation the *Vt* was higher than that of the nonsmokers, as in the other regions, but was not significantly different. Staley et al. have shown similar findings (*13*). In addition, it has been reported in a study of mice that nicotine-induced increases in nicotinic receptor numbers do not increase to the same degree in all brain regions (*30*). Moreover, the nicotinic receptor is more abundant in the thalamus, with greater receptor heterogeneity, than in other brain regions (*19*). However, the characteristics of the acute response of neuronal nAChRs to nicotine depend on their subunit composition (*31,32*). Nicotinic receptor subtypes are affected differentially by chronic exposure to nicotine, both in cell models (*33–35*) and in vivo (*35*). Multiple factors are thought to be responsible for these differences.

This study should be interpreted in the context of several limitations. (a) The number of subjects evaluated was small, which reduced the statistical accuracy. (b) The study design used did not allow us to deal with a within-subject analysis of the whole group, as the variables were analyzed independently. (c) The smokers varied in their rate and depth of inhalation of smoke, and these interindividual

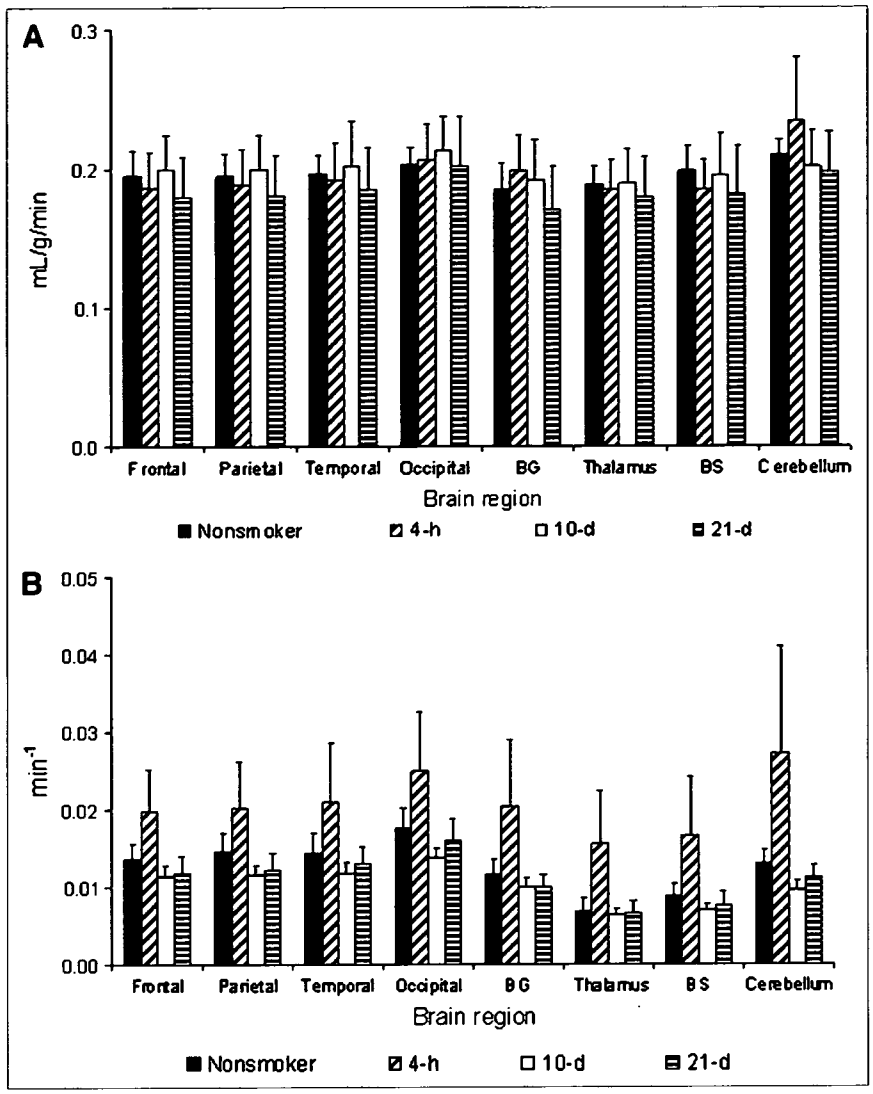

FIGURE 3. Temporal changes in rate constants K_1 and k_2 in nonsmokers and smokers after smoking cessation. (A) Rate constant K_1 (mL/g/min). (B) Rate constant k_2 (min^{-1}). BG = basal ganglia; BS = brain stem.

differences could have affected our measurements. (d) The detection limit of the plasma nicotine measurements was not enough to evaluate all blood samples. Thus, we were not able to correlate the plasma nicotine/cotinine levels with *Vt*. (e) We have not coregistered SPECT images with MRI, which would have been the most appropriate method for placement of ROIs. (f) We have not evaluated the smoker's behavior during the smoking-cessation period. We believe that the nicotine binding and desensitization of the nAChRs in the brain alleviate the cigarette craving and that craving will be the worst during the first 10 d of cessation due to the upregulation of nAChRs. The craving process should minimize after 21 d, as we observe similar levels of occupancy as nonsmokers at that time. However, we cannot exclude the possibility of other nAChR subtypes being involved in the process of tobacco dependence.

CONCLUSION

We have described the in vivo imaging of nAChR upregulation and recovery in response to short-term smoking cessation in smokers using ^{123}I-5IA SPECT. Our results clearly suggest that tobacco smoking is associated with an upregulation of nicotine binding sites in the brain. The upregulation of the nAChRs of the smokers after chronic exposure to nicotine was downregulated to the level in nonsmokers after ~21 d of smoking cessation. Thus, the upregulation of receptor numbers is a temporary effect. Nicotine dependence and difficulty in smoking cessation are also interesting with regard to the findings of the ^{123}I-5IA SPECT study. The decrease in nicotinic receptors to nonsmoker levels may be the breaking point during the nicotine withdrawal period.

ACKNOWLEDGMENTS

The authors thank Dr. Masanori Ichise (Department of Radiology, Columbia University, College of Physicians and Surgeons) for his tremendous editorial support and suggestions on this project. The authors also thank Nihon Medi-Physics Co. Ltd., Japan, for providing sodium ^{123}I-iodide.

This work was supported in part by a grant from the Research for the Future Program of the Japan Society for the Promotion of Science (JSPS-RFTF97K00201); Grants-in-Aid for Scientific Research from the Ministry of Education, Science and Technology of Japan; a research grant from Longevity Sciences from the Ministry of Health and Welfare; and a grant from the Smoking Research Foundation.

REFERENCES

1. Gotti C, Fornasari D, Clementi F. Human neuronal nicotinic receptors. *Prog Neurobiol.* 1997;53:199–237.
2. Paterson D, Nordberg A. Neuronal nicotinic receptors in the human brain. *Proc Neurobiol.* 2000;61:75–111.
3. Shimohama S, Kihara T. Nicotinic receptor-mediated protection against beta-amyloid neurotoxicity. *Biol Psychiatry.* 2001;49:233–239.
4. Decker MW, Rueter LE, Bitner RS. Nicotinic acetylcholine receptor agonists: a potential new class of analgesics. *Curr Top Med Chem.* 2004;4:369–384.
5. Buisson B, Bertrand D. Nicotine addiction: the possible role of functional up-regulation. *Trends Pharmacol Sci.* 2002;23:130–136.
6. Pietila K, Lahde T, Attila M, Ahtee L, Nordberg A. Regulation of nicotinic receptors in the brain of mice withdrawn from chronic oral nicotine treatment. *Naunyn Schmiedebergs Arch Pharmacol.* 1998;357:176–182.
7. Rowell PP, Li M. Dose-response relationship for nicotine-induced up-regulation of rat brain nicotinic receptors. *J Neurochem.* 1997;68:1982–1989.
8. Collins AC, Romm E, Wehner JM. Dissociation of the apparent relationship between nicotine tolerance and up-regulation of nicotinic receptors. *Brain Res Bull.* 1990;25:373–379.
9. Koylu E, Demirgoren S, London ED, Pogun S. Sex difference in up-regulation of nicotinic acetylcholine receptors in rat brain. *Life Sci.* 1997;61:L185–L190.
10. Perry DC, Davila-Garcia MI, Stockmeier CA, Kellar KJ. Increased nicotinic receptors in brains from smokers: membrane binding and autoradiography studies. *J Pharmacol Exp Ther.* 1999;289:1545–1552.
11. Teaktong T, Graham AJ, Johnson M, Court JA, Perry EK. Selective changes in nicotinic acetylcholine receptor subtypes related to tobacco smoking: an immunohistochemical study. *Neuropathol Appl Neurobiol.* 2004;30:243–254.
12. Kassiou M, Eberl S, Meikle SR, et al. In vivo imaging of nicotinic receptor upregulation following chronic (-)-nicotine treatment in baboon using SPECT. *Nucl Med Biol.* 2001;28:165–175.
13. Staley JK, Krishnan-Sarin S, Cosgrove KP, et al. Human tobacco smokers in early abstinence have higher of b2* nicotinic acetylcholine receptors than non-smokers. *J Neurosci.* 2006;26:8707–8714.
14. Breese CR, Marks MJ, Logel MJ, et al. Effect of smoking history on [^{3}H]nicotine binding in human postmortem brain. *J Pharmacol Exp Ther.* 1997; 282:7–13.
15. Saji H, Ogawa M, Ueda M, et al. Evaluation of radioiodinated 5-iodo-3-(2(S)-azetidinylmethoxy)pyridine as a ligand for SPECT investigations of brain nicotinic acetylcholine receptors. *Ann Nucl Med.* 2002;16:189–200.
16. Musachio JL, Scheffel U, Finley PA, et al. 5-[I-125/123]Iodo-3(2(S)-azetidinylmethoxy)pyridine, a radioiodinated analog of A-85380 for in vivo studies of central nicotinic acetylcholine receptors. *Life Sci.* 1998;62:351–357.
17. Ueda M, Iida Y, Mukai T, et al. 5-[^{123}I]Iodo-A-85380: assessment of pharmacological safety, radiation dosimetry and SPECT imaging of brain nicotinic receptors in healthy human subjects. *Ann Nucl Med.* 2004;18: 337–344.
18. Vaupel DB, Tella SR, Huso DL, et al. Pharmacology, toxicology, and radiation dosimetry evaluation of [I-123]5-I-a-85380, a radioligand for in vivo imaging of cerebral neuronal nicotinic acetylcholine receptors in humans. *Drug Dev Res.* 2003;58:149–168.
19. Mamede M, Ishizu K, Ueda M, et al. Quantification of human nicotinic acetylcholine receptors with ^{123}I-5IA SPECT. *J Nucl Med.* 2004;45:1458–1470.
20. Marks MJ, Pauly JR, Gross SD, et al. Nicotine binding and nicotinic receptor subunit RNA after chronic nicotine treatment. *J Neurosci.* 1992;12:2765–2784.
21. Peng X, Gerzanich V, Anand R, Whiting PJ, Lindstrom J. Nicotine-induced increase in neuronal nicotinic receptors results from a decrease in the rate of receptor turnover. *Mol Pharmacol.* 1994;46:523–530.
22. Marks MJ, Burch JB, Collins AC. Genetics of nicotine response in four inbred strains of mice. *J Pharmacol Exp Ther.* 1983;226:291–302.
23. Bencherif M, Fowler K, Lukas RJ, Lippiello PM. Mechanisms of up-regulation of neuronal nicotinic acetylcholine receptors in clonal cell lines and primary cultures of fetal rat brain. *J Pharmacol Exp Ther.* 1995;275:987–994.
24. Broussolle EP, Wong DF, Fanelli FJ, London ED. In vivo specific binding of [^{3}H]l-nicotine in the mouse brain. *Life Sci.* 1989;44:1123–1132.
25. Muzic R, Berridge M, Friedland R, Zhu N, Nelson A. PET quantification of specific binding of carbon-11-nicotine in human brain. *J Nucl Med.* 1998;39: 2048–2054.
26. Brody AL, Mandelkern MA, London ED, et al. Cigarette smoking saturates brain α4β2 nicotinic acetylcholine receptors. *Arch Gen Psychiatry.* 2006;63: 907–915.
27. Ding Y-S, Volkow ND, Logan J, et al. Occupancy of brain nicotinic acetylcholine receptors by nicotine doses equivalent to those obtained when smoking a cigarette. *Synapse.* 2000;35:234–237.
28. Collins AC, Bhat RV, Pauly JR, Marks MJ. Modulation of nicotine receptors by chronic exposure to nicotinic agonists and antagonists. *Ciba Found Symp.* 1990; 152:68–82.
29. Marks MJ, Stitzel JA, Collins AC. Time course study of the effects of chronic nicotine infusion on drug response and brain receptors. *J Pharmacol Exp Ther.* 1985;235:619–628.
30. Collins AC, Marks MJ, Pauly JR. Differential effect of chronic nicotine treatment on nicotinic receptor numbers in various brain regions of mice. *J Subst Abuse.* 1989;1:273–286.
31. Luetje CW, Patrick J. Both α and β subunits contribute to the agonist sensitivity of neuronal acetylcholine receptors. *J Neurosci.* 1991;11:837–845.
32. Fenster CP, Rains MF, Noerager B, Quick MW, Lester RAJ. Influence of subunit composition on desensitization of neuronal acetylcholine receptors at low concentrations of nicotine. *J Neurosci.* 1997;17:5747–5759.
33. Hsu Y-N, Amin J, Weiss DS, Wecker L. Sustained nicotine exposure differentially affects α3β2 and α4β2 neuronal nicotinic receptors expressed in *Xenopus* oocytes. *J Neurochem.* 1996;66:667–675.
34. Olale F, Gerznich V, Kurytov A, Wang F, Lindstrom J. Chronic nicotine exposure differentially affects the function of human α3, α4 and α7 neuronal nicotinic receptor subtypes. *J Pharmacol Exp Ther.* 1997;283:675–683.
35. Peng X, Gerzanich V, Anand R, Wang F, Lindstrom J. Chronic nicotine treatment up-regulates α3 and α7 acetylcholine receptor subtypes expressed by the human neuroblastoma cell line SH-SY5Y. *Mol Pharmacol.* 1997;51:776–784.

ELSEVIER

Journal of the Neurological Sciences 256 (2007) 52–60

Journal of the Neurological Sciences

www.elsevier.com/locate/jns

Quantification of nicotinic acetylcholine receptors in Parkinson's disease with ^{123}I-5IA SPECT

Naoya Oishi [a], Kazuo Hashikawa [a], Hidefumi Yoshida [a,b], Koichi Ishizu [c], Masashi Ueda [d,e], Hidekazu Kawashima [c], Hideo Saji [d], Hidenao Fukuyama [a,*]

[a] *Human Brain Research Center, Kyoto University Graduate School of Medicine, 54 Kawahara-cho, Shogoin, Sakyo-ku, Kyoto 606-8507, Japan*
[b] *Department of Rehabilitation Medicine, Shiga Medical Center for Adults, Shiga, Japan*
[c] *Department of Nuclear Medicine and Diagnostic Imaging, Kyoto University Graduate School of Medicine, Kyoto, Japan*
[d] *Department of Patho-Functional Bioanalysis, Kyoto University Graduate School of Pharmaceutical Science, Kyoto, Japan*
[e] *Radioisotope Laboratory, Kyoto Prefectural University of Medicine, Kyoto, Japan*

Received 12 September 2006; received in revised form 20 December 2006; accepted 6 February 2007
Available online 23 March 2007

Abstract

We quantified *in vivo* brain nicotinic acetylcholine receptor (nAChR) distributions in patients with Parkinson's disease (PD) and evaluated correlations between nAChR distributions and clinical variables of the patients, especially dopaminergic medications. Ten patients with PD without dementia underwent 5-^{123}I-iodo-3-(2(*S*)-azetidinylmethoxy)pyridine (^{123}I-5IA) single photon emission computed tomography (SPECT) and the data were compared with those of 10 age-matched healthy volunteers. Correlation analyses between ^{123}I-5IA distribution volumes (DVs) in each brain region and clinical variables of the patients were also performed. The PD group showed a statistically significant decrease (20–25%) in the brainstem and frontal cortex as compared with the control group. Although age, duration of disease, daily dose of levodopa, duration of PD medication use, and scores on the motor section of Unified Parkinson's Disease Rating Scale were not significantly correlated with DV values in any brain regions, high daily doses of dopamine agonist showed a significant negative correlation with DVs in the cerebellum, and temporal, parietal and occipital cortices. These findings suggest that patients with PD without dementia can show reductions especially in the brainstem and frontal cortex. They also suggest that dopamine agonists can have a negative influence on the distribution of nAChRs.

Keywords: Parkinson's disease; Single photon emission computed tomography; 5-123I-iodo-3-(2(*S*)-azetidinylmethoxy)pyridine; Nicotinic acetylcholine receptors; Distribution volume; Dopamine agonist

1. Introduction

Parkinson's disease (PD) is a movement disorder characterized by a progressive decline in nigrostriatal dopaminergic function. Although the primary deficit seems a loss of substantia nigra dopaminergic neurons, other neurotransmitter systems are also affected, including the nicotinic cholinergic system [1]. Extensive evidence now indicates that there are significant declines in nicotinic acetylcholine receptors (nAChRs) in the post-mortem brains of both demented and non-demented patients with PD [2,3].

nAChRs are a family of ligand-gated ion channels composed of multiple α (α_2–α_7) and β (β_2–β_4) subunits and the majority of high affinity nAChRs in the brain comprise the $\alpha_4\beta_2$ subtype [1]. Most brain nAChRs are presynaptic and their most important function is to modulate the release of various neurotransmitters such as dopamine, acetylcholine, gamma-aminobutyric acid (GABA), and glutamate [4,5]. nAChRs are implicated in memory, attention, and reward [1]. Furthermore, numerous studies have shown that nicotinic receptors located on presynaptic dopaminergic terminals [6] modulate the striatal release of

* Corresponding author. Tel.: +81 75 751 3695; fax: +81 75 751 3202.
E-mail address: fukuyama@kuhp.kyoto-u.ac.jp (H. Fukuyama).

0022-510X/$ - see front matter © 2007 Elsevier B.V. All rights reserved.
doi:10.1016/j.jns.2007.02.014

dopamine, which is essential for the control of movement and posture [5].

Recently, 5-iodo-3-(2(*S*)-azetidinylmethoxy) pyridine (5IA), a derivative of A-85380 iodinated at the 5-position of the pyridine ring, was reported to be a promising ligand for imaging nAChRs because of its high uptake in the mammalian brain, a distribution consistent with the known density of nAChRs, a high-affinity nAChR ligand with high subtype selectivity for $\alpha_4\beta_2$ [7]. It has been predicted that 5IA labeled with ^{123}I (^{123}I-5IA) injected at the usual clinical dose would have no pharmacological effect and that the absorbed dose of radiation appeared acceptable for clinical SPECT imaging[8]. Furthermore, the regional distribution of radioactivity in the image of healthy human brain using ^{123}I-5IA was associated with the known nAChR distribution [9,10]. Recently, Fujita et al. first reported a pilot study of in vivo nAChR imaging using 123I-5IA in PD and showed widespread significant decrease of distribution in both cortical and subcortical regions [11].

In the present study, we quantified *in vivo* brain nAChR distributions in PD patients using ^{123}I-5IA SPECT. We also evaluated correlations between nAChR distributions and clinical variables of PD patients, especially dopaminergic medications, because animal studies suggest that the dopaminergic system can exert a negative modulatory influence on nAChR expression [12].

2. Methods

2.1. Subjects

Ten patients with PD (five men and five women; mean age±S.D., 66.9±7.0 years) were enrolled in this study. Diagnosis was made by movement disorder subspecialists based on the UK Brain Bank criteria [13]. None of the subjects had a history of smoking or cholinergic medications, which could have a strong influence on nAChR distributions. Demented patients defined by DSM-IV criteria [14] and a Mini-Mental State Examination (MMSE) score [15] of 25 or less were excluded. Patients with hallucination episodes were also excluded. MRI showed no brain morphological abnormalities in all patients. Clinical assessment of each PD patient was performed with the motor section of the Unified Parkinson's Disease Rating Scale (UPDRS), [16] Hoehn and Yahr scale [17] and MMSE scores (Table 1). Two types of dopamine agonists were used in the patients, and the doses were calculated relative to bromocriptine according to the formula: bromocriptine 10 mg=pergolide 550 μg=cabergoline 2 mg [18]. All patients underwent clinical assessments and SPECT at least 12 h after they took their last anti-parkinsonian medications.

^{123}I-5IA SPECT data were compared between patients and 10 healthy volunteers without any history of smoking, cholinergic medications, or neurologic or psychiatric illness (seven men and three women; age, 65.8±10.2 years). There was no significant difference in age (p=0.78 by two-tailed Student's t-test) or gender (p=0.65 by Pearson's chi-square test) between the two groups. All subjects gave written informed consent based on the study protocol approved by the Ethics Committee of Kyoto University School of Medicine.

2.2. Radiochemistry

5IA and 5-(tri-*n*-butylstannyl)-3-(1-*tert*-butoxycarbonyl-2(*S*)-azetidinylmethoxy)pyridine, the stannyl precursor of ^{123}I-5IA, was synthesized according to a previous report [7]. No carrier-added sodium ^{123}I-iodine was supplied by Nihon

Table 1
Clinical features in patients with Parkinson's disease

No.	Age (years)	Sex	Disease duration (years)	H-Y scale	UPDRS III	MMSE	Daily levodopa (mg)	Daily agonist* (mg)	Drug duration (years)	PD medications (mg)
1	77	M	1.0	2.0	17	28	100	0	0.7	Levodopa/DCI 100
2	57	M	8.2	5.0	40	26	600	15.0	7.6	Levodopa/DCI 600, cabergoline 3, amantadine 125, droxidopa 600
3	74	F	1.8	2.0	14	27	300	1.3	0.3	Levodopa/DCI 300, cabergoline 0.25, pergolide 0.2
4	69	F	0.5	2.5	15	29	0	0	0.0	Amantadine 100
5	55	F	6.8	4.0	21	30	400	42.7	6.4	Levodopa/DCI 400, cabergoline 4, pergolide 1.25
6	67	F	2.9	1.0	11	29	100	20.0	1.9	Levodopa/DCI 100, cabergoline 4, amantadine 150
7	72	M	7.2	2.0	12	30	300	13.6	4.6	Levodopa/DCI 300, pergolide 0.75, amantadine 150
8	66	M	4.4	2.0	6	29	400	20.0	2.3	Levodopa/DCI 400, cabergoline 4
9	63	F	1.1	1.0	7	29	200	13.6	1.0	Levodopa/DCI 200, pergolide 0.75
10	69	M	3.3	2.0	19	30	200	1.8	2.8	Levodopa/DCI 200, pergolide 0.1
Mean	66.9		3.7	2.4	16.2	28.7	260	12.8	2.8	
S.D.	7.0		2.8	1.2	9.6	1.3	178	13.3	2.6	

DCI=dopa-decarboxylase inhibitor; H-Y=Hoehn and Yahr; MMSE=Mini-Mental State Examination; PD=Parkinson's disease; UPDRS III=the motor section of the Unified Parkinson's Disease Rating Scale.

* The dosages of two types of dopamine agonists (pergolide, cabergoline) were calculated relative to bromocriptine.

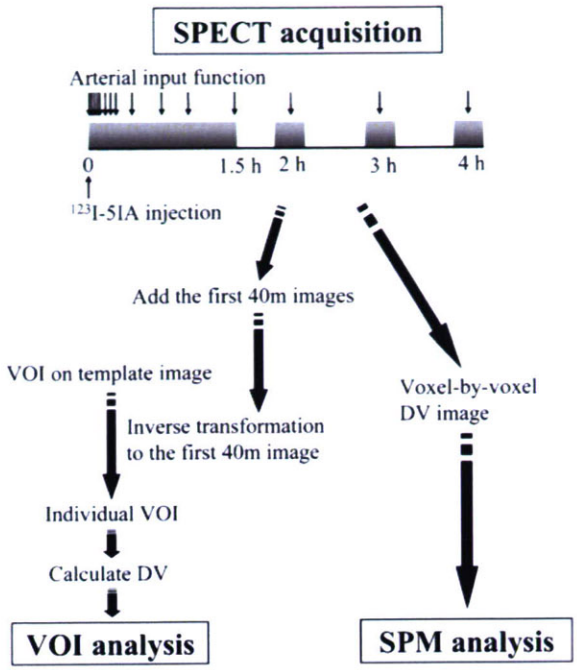

Fig. 1. Simple methodological diagram demonstrating the steps involved in SPECT acquisition and analysis.

Medi-Physics Co. Ltd. (Nishinomiya, Japan). Radiolabeling was also performed according to previous reports [7,8,10]. Radiochemical purity was >98% and the specific activity determined from the ultraviolet absorbance at 254 nm was >169 GBq/μmol.

2.3. SPECT acquisition

All SPECT dynamic scans were acquired with a triple-head rotating γ-camera system (PRISM 3000; Picker International, Inc.) equipped with low-energy, high resolution, fanbeam collimators. This system provides a spatial resolution of 8.0-mm full width at half maximum (FWHM) at the center of the field of view with a sensitivity of 135 cps/MBq. ^{123}I-5IA was administered intravenously to subjects, over a period of 1 min at a constant rate with an infusion pump. There is no significant difference in the dose of ^{123}I-5IA between the two groups, as shown by two-tailed Student's *t*-test (175±13.8 MBq in the PD group and 183±32.5 MBq in the control group; $p=0.49$). The scan was started simultaneously with the injection. Data acquisition was performed in 64×64 matrices in a continuous rotation mode with 40 steps for 120° and 1.5 s per step, which translates to a 1 min for 1 SPECT dataset. All subjects underwent a 90-min scan after intravenous injection of ^{123}I-5IA, followed by three sets of 20-min scan (at 2, 3, and 4 h after the injection) (Fig. 1). All SPECT images were filtered with a Butterworth filter (cutoff frequency, 0.25; order, 4), and reconstructed using a filtered backprojection algorithm with a ramp filter. Attenuation correction was performed using ellipses outer line approximation and Chang's method (coefficient of 0.06/cm) adjusted for each slice. The same ellipse size was kept for the different scans of each subject. Scatter correction was not applied.

An arterial input function was obtained for each subject. Twenty-four arterial blood samples were drawn, initially every 10 s during the first two min, followed by every 15 s during the next minute, and then subsequently at 5, 7, 10, 20, 30, 45, 60 and 90 min. Additionally, three venous blood samples were obtained at 2, 3, and 4 h after injection because we previously confirmed that venous blood sampling was a simple and acceptable choice for input function at several time points, including 2, 3, and 4 h after injection [10]. Fourteen samples (1, 2, 3, 5, 7, 10, 20, 30, 45, 60, 90, 120, 180, and 240 min) were analyzed for metabolite determination. Metabolite correction was performed using the same method as the previously reported [10].

2.4. Image analysis by automated volume of interest

All SPECT images of each subject were coregistered to each other using Statistical Parametric Mapping (SPM) version 2 (Wellcome Department of Cognitive Neurology, UCL, London, UK) implemented in Matlab 6.5 (Math

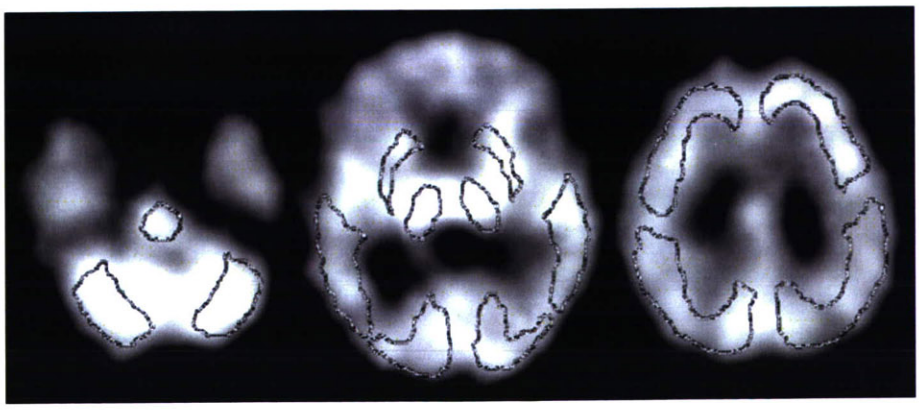

Fig. 2. SPECT images of a healthy volunteer which show radioactivity collected 0 to 40 min after injection of ^{123}I-5-iodo-3-(2(*S*)-azetidinylmethoxy) pyridine, and the volumes of interest (VOIs). VOIs were placed in the thalamus, striatum, brainstem, cerebellum, and the frontal, temporal, parietal, and occipital cortices.

Works, Natick, Mass., USA). The ^{123}I-5IA images during the first 40 min were added to create images with good delineation of cerebral cortices [9]. The manually traced template image during the first 40 min was created using high-resolution 3D T1-weighted magnetic resonance (MR) images in three healthy volunteers. Using SPM, the MR images were coregistered to each SPECT image during the first 40 min, and both MR and SPECT images were spatially normalized to a standard anatomic orientation (Montreal Neurological Institute [MNI] space) by obtaining parameters from MR images. Then, the template SPECT image during the first 40 min was generated by averaging these three normalized images. Volumes of interest (VOIs) were placed on the template MR image overlying the thalamus, striatum, brainstem, cerebellum, and frontal, temporal, parietal, and occipital cortices. The standard VOIs were transformed to individual images by SPM using the 'Invert deformations' function (Fig. 2). Since these individual VOIs are automatically defined, the operator induced bias in defining VOIs manually can be avoided.

A two-compartment model was applied to calculate distribution volumes (DVs) in each VOI according to previous reports [10]. Non-linear least-squares analysis was performed on the VOI generated time-activity data using PMOD 2.61. The model configuration was implemented to account for the contribution from activity in the cerebral blood volume. Cerebral blood volume was assumed to be 5% of brain volume [9,10]. The accuracy of DV was evaluated by a percentage of the rate constants (coefficient of variation, %COV) in each brain region [9].

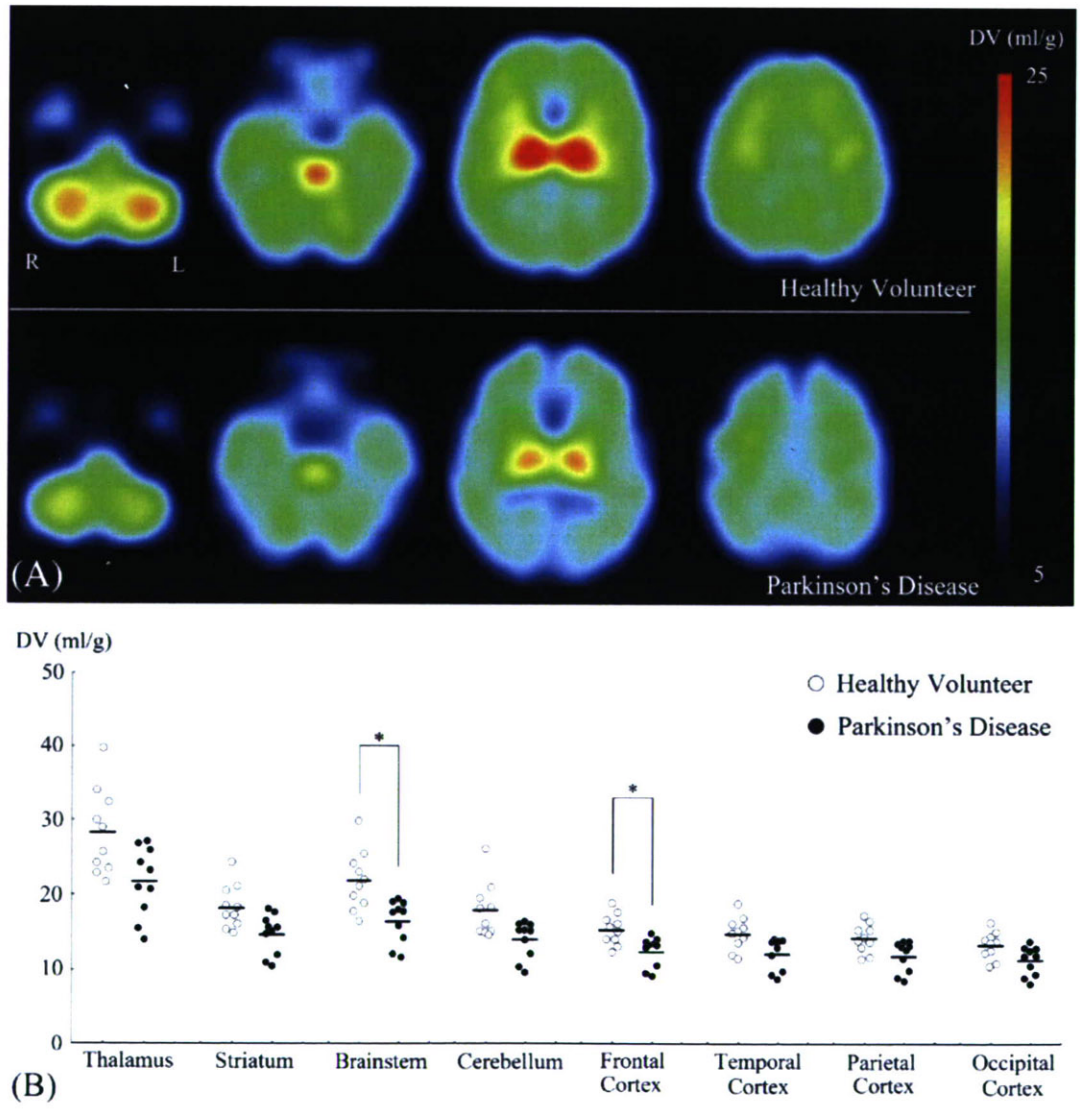

Fig. 3. (A) Averaged ^{123}I-5IA distribution volume (DV) images of the control group (upper) and the Parkinson's disease (PD) group (lower) after spatial normalization by Statistical Parametric Mapping (SPM). Visual inspection of these images revealed lower DVs in the PD group compared with the control group. (B) Scatter diagrams showing ^{123}I-5IA distribution volumes in each volume of interest in healthy volunteers and PD patients. * $p<0.05$ after Bonferroni correction for multiple comparisons ($n=8$).

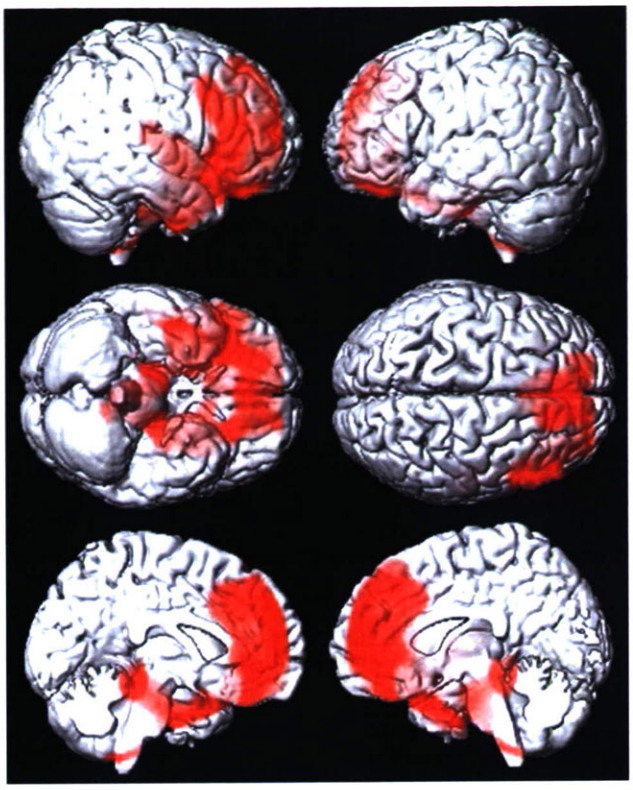

Fig. 4. Statistical parametric maps of significant ^{123}I-5IA distribution volume decrease in the Parkinson's disease group as compared with the control group, superimposed on a surface-rendered MRI template.

2.5. Image analysis by Statistical Parametric Mapping

The method of analysis using SPM, allowing exploratory voxel by voxel group comparisons throughout the entire brain volume without requiring an *a priori* hypothesis, was also used in this study. The voxel-by-voxel DV images were calculated using graphical methods of analysis [19]. The voxel-by-voxel images of the delivery of the radioligand (K_1) were also calculated using PMOD [20]. Using SPM, ^{123}I-5IA DV images during the first 40 min were coregistered to each of the DV images, and both images were spatially normalized to the MNI space by obtaining parameters from images during the first 40 min. The template DV image was generated by averaging the normalized images and smoothed with an isotropic Gaussian kernel. Each DV image was transformed into the template DV image and smoothed by three-dimensional convolution with an isotropic Gaussian kernel (FWHM = 10 mm). The normalized DV images were compared by voxel-by-voxel contrasts using *t* statistics between the two groups [21]. As DV values are quantitative, all SPM analyses were performed without global normalization. The K_1 images were also compared by the same way as the DV images.

Correlation analyses between the voxel-by-voxel DV images and clinical variables of interest in PD patients were also performed for each voxel using the general linear approach [21].

Brain regions (approximate Brodmann areas) were estimated based on the methods of Talairach and Tournoux, [22] after adjustment (www.mrc-cbu.cam.ac.uk/Imaging/mnispace.html) for differences between MNI and Talairach coordinates. SPM maps thresholded at $Z > 3.09$ ($p < 0.001$) were obtained and only those at $p < 0.05$, cluster-level corrected for multiple comparisons, were considered significant.

2.6. Statistical analysis

The ^{123}I-5IA DV values of each automated VOI were analyzed using one-way analysis of variance (ANOVA) and post hoc Bonferroni correction for the PD group and the control group. Differences were considered significant at $p < 0.05$.

Differences in ^{123}I-5IA DV values of each automated VOI between the PD group and the control group were analysed using two-tailed Student's *t*-test with Bonferroni correction for multiple comparisons. Because of the multiple comparisons in eight brain areas, differences between the groups were considered significant at a level of $p < 0.00625$ (=0.05/8).

3. Results

3.1. Image analysis by automated volume of interest

In all brain regions, DVs were well identified with %COV values of 0.87% to 2.2%. The highest DVs were found in the

Table 2
Brain regions of significant ^{123}I-5IA distribution volume decrease in the Parkinson's disease group as compared with the control group in Statistical Parametric Mapping (SPM) analyses

Cluster-level		Region (BA)	Coordinate			*Z* score
			Talairach space			
Corrected *P*	*k*		*x*	*y*	z	
<0.001	28854	R Medial Frontal Gyrus (8, 10)	6	49	1	3.83
		R Middle Frontal Gyrus (9)	51	15	34	3.78
		R Inferior Frontal Gyrus (45, 47)	32	27	−8	3.74
		Anterior Cingulate Gyrus (32)	0	23	28	3.72
		L Uncus (38)	−14	−7	−33	3.85
		R Superior Temporal Gyrus (22)	46	−8	−1	3.54
		R Orbital Gyrus (11)	20	38	−24	3.54
		L Medial Frontal Gyrus (8)	−8	45	36	3.49
		R Pons	12	−17	−23	3.45
		L Superior Frontal Gyrus (11)	−16	49	−21	3.39
		L Midbrain	−2	−35	−5	3.37
		L Middle Frontal Gyrus (11)	−18	44	−22	3.37
		L Orbital Gyrus (47)	−16	34	−24	3.35
		L Inferior Frontal Gyrus (11, 47)	−22	26	−20	3.31

Each of the regions had a local peak *Z* score within the clusters. BA = Brodmann area; *k* = number of activated voxels; L = left; R = right.

thalamus (ANOVA, $p<0.001$) in both groups (Fig. 3). Subsequently, the brainstem, cerebellum, and striatum were assembled in a group of moderate DVs in both groups. No significant differences were observed between them. DVs of the brainstem were significantly higher than those of any cortical regions in the control group, whereas DVs of the brainstem were significantly higher than those of the temporal, parietal, and occipital cortices in the PD group. The cortical regions were arranged in a group of low DV values in both groups and no significant differences were observed between them.

In the PD group, there was a reduction of DV by 15% to 25% in each region compared with the control group. The PD group showed a tendency for DV reduction in the thalamus, striatum, cerebellum, and the temporal, parietal and occipital cortices and a significant decrease in the brainstem and the frontal cortex compared with the control group.

3.2. Image analysis by Statistical Parametric Mapping

The PD group showed neither significantly increased nor decreased K_1 in any region compared with the control group. The statistical parametric maps of DV decrease in the PD group compared with the control group are shown in Fig. 4 and Table 2. The PD group showed significantly reduced DV in the frontal areas including the superior, middle and inferior frontal gyri, the anterior cingulate gyrus, the medial frontal gyrus and the orbital gyrus; in the temporal areas including the superior temporal gyrus and the uncus; and in the brainstem areas including the midbrain and pons. No regions revealed significantly higher DV values in the PD group than in the control group. These results were generally consistent with the automated VOI analyses.

3.3. Correlations between DVs and clinical variables of PD patients

Age, duration of disease, daily dose of levodopa, duration of PD medication, and the scores of the motor section of UPDRS were not significantly correlated with the voxel-by-voxel DV images. In contrast, the daily dose of dopamine agonist showed a significant negative correlation with DV in the cerebellar areas including the cerebellar hemisphere; in the temporal areas including the superior, middle and inferior temporal gyri, the fusiform gyrus and the parahippocampal gyrus; in the parietal areas including the supramarginal gyrus, the inferior parietal lobule and the postcentral gyrus; and in the occipital areas including the superior, middle and inferior

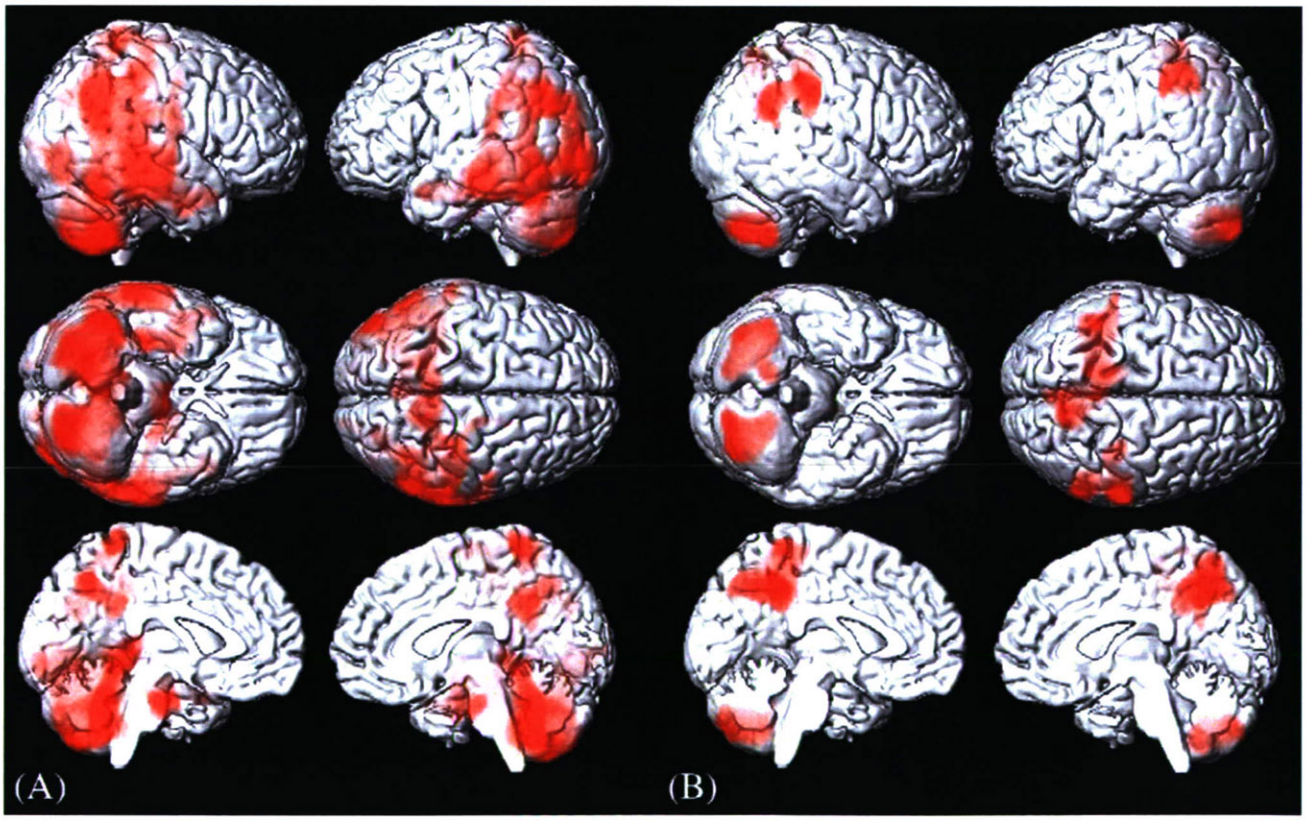

Fig. 5. (A) Statistical parametric maps of significantly negative correlation between the ^{123}I-5IA distribution volume (DV) images and daily dose of dopamine agonist in patients with Parkinson's disease (PD), superimposed on a surface-rendered MRI template. (B) Statistical parametric maps of significantly negative correlation between the ^{123}I-5IA DV images and daily dose of dopamine agonist in PD patients after age was inserted as a 'nuisance' variable on Statistical Parametric Mapping (SPM) analyses.

Table 3
(A) Brain regions of significantly negative correlations between the voxel-by-voxel ^{123}I-5IA distribution volume (DV) images and daily dose of dopamine agonist in patients with Parkinson's disease (PD) in Statistical Parametric Mapping (SPM) analyses

Cluster-level		Region (BA)	Coordinate			Z score
			Talairach space			
Corrected P	k		x	y	z	
<0.001	47408	R Cerebellar Hemisphere	42	−52	−38	4.15
		L Cerebellar Hemisphere	−26	−74	−38	3.92
		R Middle Temporal Gyrus (21)	65	−33	−2	3.91
		L Lingual Gyrus (19)	−16	−43	−1	3.89
		R Superior Temporal Gyrus (39)	59	−57	27	3.84
		L Middle Occipital Gyrus	−38	−87	−1	3.80
		L Superior Occipital Gyrus (19)	−46	−78	30	3.77
		L Fusiform Gyrus (37)	−49	−57	−16	3.76
		L Supramarginal Gyrus (40)	−53	−57	34	3.73
		L Inferior Temporal Gyrus (37)	−57	−55	−7	3.69
		R Inferior Temporal Gyrus (20)	53	−53	−12	3.64
		L Middle Temporal Gyrus (21)	−63	−26	−12	3.63
		R Postcentral Gyrus (5)	6	−41	68	3.58
		L Postcentral Gyrus (5)	−2	−41	67	3.55
		R Inferior Occipital Gyrus (19)	34	−78	−1	3.51
		R Parahippocampal Gyrus (36)	32	−28	−24	3.48
		L Inferior Parietal Lobule (40)	−46	−39	41	3.47
		R Inferior Parietal Lobule (40)	51	−27	46	3.40

(B) Brain regions of significantly negative correlations between the voxel-by-voxel ^{123}I-5IA DV images and daily dose of dopamine agonist in PD patients in SPM analyses after age was inserted as a 'nuisance' variable on SPM analyses

Cluster-level		Region (BA)	Coordinate			Z score
			Talairach space			
Corrected P	k		x	y	z	
<0.001	5177	L Inferior Parietal Lobule (40)	−44	−38	46	3.89
		R Precuneus (7)	10	−59	55	3.77
		L Postcentral Gyrus (3)	−16	−38	61	3.58
		L Cingulate Gyrus (31)	−4	−41	33	3.48
		R Postcentral Gyrus (5)	6	−43	63	3.10
0.010	2056	L Cerebellar Hemisphere	−28	−75	−33	3.80
0.012	1927	R Postcentral Gyrus (1, 3)	61	−25	38	3.78
		R Supramarginal Gyrus (40)	53	−49	34	3.61
		R Superior Temporal Gyrus (22)	67	−48	19	3.21
0.009	2151	R Cerebellar Hemisphere	40	−56	−38	3.57

Each of the regions had a local peak Z score within the clusters. BA = Brodmann area; k = number of activated voxels; L = left; R = right.

occipital gyri, the lingual gyrus (Fig. 5A and Table 3A). No regions showed a significant positive correlation between the daily dose of dopamine agonist and the DVs.

Correlation analyses betweenthe voxel-by-voxel DV images and the daily doses of dopamine agonist were also done by SPM with age as a 'nuisance' variable (Fig. 5B and Table 3B) because a loss of nicotine binding has been seen during aging in normal human subjects [23] and age could have a confounding effect on the distribution of nAChRs. There was a significant negative correlation between the daily dose of dopamine agonist and DV in the parietal areas including the inferior parietal lobule, the precuneus, the postcentral gyrus, the posterior cingulate gyrus and the supramarginal gyrus; in the cerebellar areas including the cerebellar hemisphere; and in the temporal areas including the superior temporal gyrus. No regions revealed significantly positive correlations between the daily dose of dopamine agonist and DV.

4. Discussion

Automated VOI analyses revealed that ^{123}I-5IA DV in all brain regions tended to be lower in the PD group compared with the age-matched control group. The result is generally consistent with previous post-mortem ^{125}I-5IA studies of nAChR distribution in PD [2] and a study of nAChR distribution in living PD patients [11]. Furthermore, the PD group showed a significant decrease of ^{123}I-5IA DV in the brainstem and frontal cortex compared with the control group. Although the decreases seem to be greater than those in the previous study [11], they may be caused by the differences of SPECT procedures, intervals of arterial sampling obtained for the first 2 min and plasma analysis. The effect of antiparkinsonian medication may result the discrepancies because the patients stopped anti-parkinsonian medication 12 h before SPECT in this study, while they continued it during SPECT [11]. The discrepancies of the brainstem may be due to the definition of the VOI in the brainstem. The VOI was placed not only in the pons but also in the midbrain in this study, while they placed the VOI only in the pons [11]. It is also possible that brain atrophy can partially influence ^{123}I-5IA DV because a recent volumetric MRI analysis showed that reduced volume in PD patients without dementia, in the frontal lobe [24]. Another limitation of this study is the small number of subjects and a low statistical power might cause no significant differences in the striatum or thalamus which were closely linked to the basal ganglia circuits. Although the previous post-mortem ^{125}I-5IA study showed a more decrease in the striatum [2], the decrease did not reach statistical significance in this study as well as in the previous study [11]. Explanation for the discrepancy may be different disease severity. Their study was a post-mortem study and the mean age in the PD group of the study was about 10 years older than that of this study [2], which suggested that disease severity was greater in their study. Low spatial resolution of SPECT might also confound the results. Further studies combined with volumetric MRI analysis or partial volume correction in larger subjects are needed to confirm these possibility. Cholinergic neurons can be found in the tegmental pedunculopontine (PPN) and laterodorsal nuclei (LDN) with important projections to the substantia nigra pars compacta (SNc), thalamus, striatum and

prefrontal cortex [1,25] and the PPN-LDN cholinergic system is affected in PD [25]. In PD patients, a decrease in high-affinity nAChRs density by 70% in the SNc and 40% to 50% in the LDN was reported [26]. Dysfunction in the PPN-LDN cholinergic system could explain the significant decrease of ^{123}I-5IA DV in the brainstem of PD patients.

It is interesting that PD patients without dementia showed a significant decrease of ^{123}I-5IA DV in the frontal cortex. PD patients show characteristic cognitive declines even in the early stage, and they show particular impairment on neuropsychologic tests sensitive for frontal lobe function[27]. Basal forebrain cholinergic pathways have impaired cholinergic innervations in PD patients and the nucleus basalis of Meynert (nbM) diffusely projects to the neocortex, particularly the frontal and parietal cortices, and the amygdala [28]. Previous post-mortem studies showed a decreased number of nAChRs in the frontal, temporal, parietal and occipital cortices in both demented and non-demented PD [3]. The dysfunction in the nbM cholinergic system could also explain the significant decrease of ^{123}I-5IA DV in the frontal cortex in the PD group in this study. It is also possible that the decrease in the ^{123}I-5IA DV in the frontal cortex is caused by dysfunction of cholinergic interneurons in the frontal cortex. Further studies are needed to confirm this possibility because no neuropsychologic tests sensitive for frontal lobe function were used in this study.

The VOI results in this study are supported by SPM analyses which localized significant decreases in ^{123}I-5IA DV at the voxel level in spatially normalized datasets. In accordance with the previous report [11], the PD group showed neither significantly increased nor decreased K_1 in any region compared with the control group, which suggested that decreased DV in the PD group was not due to decreased local perfusion. Additionally, by using SPM, we were able to identify foci of decreased ^{123}I-5IA DV in the orbitofrontal, anterior cingulate and anterior temporal cortices. Dopaminergic projections from the midbrain, especially the SNc and the ventral tegmental area, to the orbitofrontal, anterior cingulate and anterior temporal cortices form part of the mesocorticolimbic dopaminergic system which is involved in motor, cognitive and behavourial functions [29]. Not only nigrostriatal but also mesocorticolimbic dopamine transporter density, which corresponds with presynaptic dopaminergic function, is decreased even in early PD [30]. Several studies in PD patients have shown the importance of the interaction between acetylcholine and dopamine neurotransmission[4]. In the prefrontal cortex, $\alpha_4\beta_2$ appears to play a major role in nAChR-mediated ^{3}H-dopamine release [31]. Therefore, decreased nAChRs in the orbitofrontal, anterior cingulate and anterior temporal cortices could decrease dopamine release to these regions and cause the mesocorticolimbic dysfunction.

Correlation analyses showed that age, duration of disease, and scores on the motor section of the UPDRS were not significantly correlated with DV values in any brain regions. Because clinical ratings were measured 12 h after stopping anti-parkinsonian medications, this period might be too short to determine their clinical off status and to allow for adequate correlation analyses, especially for those five patients who received cabergoline with long half-life. Although previous non-human primate studies showed that 2 weeks of levodopa treatment reduced striatal nAChRs [12] and that longer courses of levodopa treatment caused greater declines in ^{125}I-5IA binding [32], the daily dose of levodopa and duration of PD medication did not show significant correlations with DV values in any brain regions. Because all patients stopped their anti-parkinsonian medications at least 12 h before SPECT, it might explain the difference. It is also possible that the small number of patients or the narrow range of clinical variables in our study might have weakened the statistical power.

High daily doses of dopamine agonist showed a significant negative correlation with DVs in the cerebellum, and temporal, parietal and occipital cortices. To our knowledge, our study first showed the relationship between nAChR distribution and dopamine agonists in PD. Because nAChR stimulation evokes the release of dopamine, it is possible that feedback regulation occurs and that the dopaminergic system can exert a negative modulatory influence on striatal nAChR expression [12]. Evidence indicates that dopamine excites cholinergic neurons mainly via D_1-like receptors and inhibits acetylcholine release via D_2 receptors [33,34]. The differences in acetylcholine modulation in dopamine receptor subtypes might explain the robust negative correlations between ^{123}I-5IA DV values and the daily dose of dopamine agonist (in contrast to levodopa). Serotonergic mechanism affected by dopamine agonists may also be important because the function of nAChR can be modified by serotonergic agents [35]. However, the negative correlation may not be conclusive because of the small number of patients in this study. Another explanation could be that these correlations simply reflect the fact that patients who require more medication are more severely affected because a 12 h period might be too short to determine their clinical off status. It could also in principle have a direct influence on 5IA kinetics or metabolism and possibly produced an artifactitious correlation between the daily dose of dopamine agonist, especially cabergoline, and ^{123}I-5IA DV values.

The ability of dopamine agonists to modulate nAChR distributions in the cerebellum, and temporal, parietal and occipital cortices is of particular interest because dopamine agonists could influence cognitive dysfunction more than levodopa [36]. Additionally, by using SPM with age as a 'nuisance' variable, we were able to identify foci of decreased ^{123}I-5IA DV in the inferior parietal lobule, precuneus and posterior cingulate cortex. These parietal regions were reported to be decreased in regional cerebral blood flow in PD with dementia [37] and might be associated with cognitive dysfunction induced by dopamine agonists.

Acknowledgements

The authors thank Sadako Kuno M.D. (Musashi Hospital, National Center of Neurology and Psychiatry, Japan) for her assistance with patient recruitment. The authors also thank Nihon Medi-Physics Co. Ltd., Japan, for providing sodium

^{123}I-iodide. This work was partly supported by Grants-in-Aid for Scientific Research (B) 14370205, and on Priority Area 18020014 from the Ministry of Education, Culture, Sports, Science and Technology, and "Aging and Health" from the Ministry of Health, Labor and Welfare.

References

[1] Gotti C, Clementi F. Neuronal nicotinic receptors: from structure to pathology. Prog Neurobiol 2004;74:363–96.
[2] Pimlott SL, Piggott M, Owens J, Greally E, Court JA, Jaros E, et al. Nicotinic acetylcholine receptor distribution in Alzheimer's disease, dementia with Lewy bodies, Parkinson's disease, and vascular dementia: in vitro binding study using 5-[(125)i]-a-85380. Neuropsychopharmacology 2004;29:108–16.
[3] Rinne JO, Myllykyla T, Lonnberg P, Marjamaki P. A postmortem study of brain nicotinic receptors in Parkinson's and Alzheimer's disease. Brain Res 1991;547:167–70.
[4] Marshall DL, Redfern PH, Wonnacott S. Presynaptic nicotinic modulation of dopamine release in the three ascending pathways studied by in vivo microdialysis: comparison of naive and chronic nicotine-treated rats. J Neurochem 1997;68:1511–9.
[5] Wonnacott S. Presynaptic nicotinic ACh receptors. Trends Neurosci 1997;20:92–8.
[6] Clarke PB, Pert A. Autoradiographic evidence for nicotine receptors on nigrostriatal and mesolimbic dopaminergic neurons. Brain Res 1985;348:355–8.
[7] Saji H, Ogawa M, Ueda M, Iida Y, Magata Y, Tominaga A, et al. Evaluation of radioiodinated 5-iodo-3-(2(*S*)-azetidinylmethoxy)pyridine as a ligand for SPECT investigations of brain nicotinic acetylcholine receptors. Ann Nucl Med 2002;16:189–200.
[8] Ueda M, Iida Y, Mukai T, Mamede M, Ishizu K, Ogawa M, et al. 5-[123I]Iodo-A-85380: assessment of pharmacological safety, radiation dosimetry and SPECT imaging of brain nicotinic receptors in healthy human subjects. Ann Nucl Med 2004;18:337–44.
[9] Fujita M, Ichise M, van Dyck CH, Zoghbi SS, Tamagnan G, Mukhin AG, et al. Quantification of nicotinic acetylcholine receptors in human brain using [123I]5-I-A-85380 SPET. Eur J Nucl Med Mol Imaging 2003;30:1620–9.
[10] Mamede M, Ishizu K, Ueda M, Mukai T, Iida Y, Fukuyama H, et al. Quantification of human nicotinic acetylcholine receptors with 123I-5IA SPECT. J Nucl Med 2004;45:1458–70.
[11] Fujita M, Ichise M, Zoghbi SS, Liow JS, Ghose S, Vines DC, et al. Widespread decrease of nicotinic acetylcholine receptors in Parkinson's disease. Ann Neurol 2006;59:174–7.
[12] Quik M, Bordia T, Okihara M, Fan H, Marks MJ, McIntosh JM, et al. L-DOPA treatment modulates nicotinic receptors in monkey striatum. Mol Pharmacol 2003;64:619–28.
[13] Hughes AJ, Ben-Shlomo Y, Daniel SE, Lees AJ. What features improve the accuracy of clinical diagnosis in Parkinson's disease: a clinicopathologic study. Neurology 1992;42:1142–6.
[14] American Psychiatric Association. Diagnostic and statistical manual of mental disorders. DSM-IV. Washington, DC: American Psychiatric Association; 1994.
[15] Folstein MF, Folstein SE, McHugh PR. "Mini-mental state". A practical method for grading the cognitive state of patients for the clinician. J Psychiatr Res 1975;12:189–98.
[16] Fahn S, Elton RL, members of the UPDRS Development Committee. Unified Parkinson's Disease Rating Scale. In: Fahn S, Marsden CD, Calne DB, Lieberman A, editors. Recent development in Parkinson's disease. Florham Park, NJ: Macmillan Health Care Information; 1987. p. 153-63.
[17] Hoehn MM, Yahr MD. Parkinsonism: onset, progression and mortality. Neurology 1967;17:427–42.
[18] Oishi N, Udaka F, Kameyama M, Sawamoto N, Hashikawa K, Fukuyama H. Regional cerebral blood flow in Parkinson disease with nonpsychotic visual hallucinations. Neurology 2005;65:1708–15.
[19] Logan J, Fowler JS, Volkow ND, Wolf AP, Dewey SL, Schlyer DJ, et al. Graphical analysis of reversible radioligand binding from time-activity measurements applied to [N-11C-methyl]-(−)-cocaine PET studies in human subjects. J Cereb Blood Flow Metab 1990;10:740–7.
[20] Alpert NM, Eriksson L, Chang JY, Bergstrom M, Litton JE, Correia JA, et al. Strategy for the measurement of regional cerebral blood flow using short-lived tracers and emission tomography. J Cereb Blood Flow Metab 1984;4:28–34.
[21] Friston KJ, Holmes AP, Worsley KJ, Poline JB, Frith CD, Frackowiak RS. Statistical parametric maps in functional imaging: a general linear approach. Hum Brain Mapp 1995;2:189–210.
[22] Talairach J, Tournoux P. Co-planar stereotaxic atlas of the human brain. Stuttgart: Thieme; 1988.
[23] Picciotto MR, Zoli M. Nicotinic receptors in aging and dementia. J Neurobiol 2002;53:641–55.
[24] Burton EJ, McKeith IG, Burn DJ, Williams ED, JT, OB. Cerebral atrophy in Parkinson's disease with and without dementia: a comparison with Alzheimer's disease, dementia with Lewy bodies and controls. Brain 2004;127:791–800.
[25] Pahapill PA, Lozano AM. The pedunculopontine nucleus and Parkinson's disease. Brain 2000;123:1767–83.
[26] Perry EK, Morris CM, Court JA, Cheng A, Fairbairn AF, McKeith IG, et al. Alteration in nicotine binding sites in Parkinson's disease, Lewy body dementia and Alzheimer's disease: possible index of early neuropathology. Neuroscience 1995;64:385–95.
[27] Taylor AE, Saint-Cyr JA, Lang AE. Frontal lobe dysfunction in Parkinson's disease. The cortical focus of neostriatal outflow. Brain 1986;109:845–83.
[28] Forgacs PB, Bodis-Wollner I. Nicotinic receptors and cognition in Parkinson's Disease: the importance of neuronal synchrony. J Neural Transm 2004;111:1317–31.
[29] Le Moal M, Simon H. Mesocorticolimbic dopaminergic network: functional and regulatory roles. Physiol Rev 1991;71:155–234.
[30] Ouchi Y, Yoshikawa E, Okada H, Futatsubashi M, Sekine Y, Iyo M, et al. Alterations in binding site density of dopamine transporter in the striatum, orbitofrontal cortex, and amygdala in early Parkinson's disease: compartment analysis for beta-CFT binding with positron emission tomography. Ann Neurol 1999;45:601–10.
[31] Cao YJ, Surowy CS, Puttfarcken PS. Different nicotinic acetylcholine receptor subtypes mediating striatal and prefrontal cortical [3H] dopamine release. Neuropharmacology 2005;48:72–9.
[32] Quik M, Vailati S, Bordia T, Kulak JM, Fan H, McIntosh JM, et al. Subunit composition of nicotinic receptors in monkey striatum: effect of treatments with 1-methyl-4-phenyl-1,2,3,6-tetrahydropyridine or L-DOPA. Mol Pharmacol 2005;67:32–41.
[33] DeBoer P, Abercrombie ED. Physiological release of striatal acetylcholine in vivo: modulation by D1 and D2 dopamine receptor subtypes. J Pharmacol Exp Ther 1996;277:775–83.
[34] Aosaki T, Kiuchi K, Kawaguchi Y. Dopamine D1-like receptor activation excites rat striatal large aspiny neurons in vitro. J Neurosci 1998;18:5180–90.
[35] Garcia-Colunga J, Miledi R. Effects of serotonergic agents on neuronal nicotinic acetylcholine receptors. Proc Natl Acad Sci U S A 1995;92:2919–23.
[36] Olanow CW, Watts RL, Koller WC. An algorithm (decision tree) for the management of Parkinson's disease (2001): treatment guidelines. Neurology 2001;56:S1–S88.
[37] Firbank MJ, Colloby SJ, Burn DJ, McKeith IG, O'Brien JT. Regional cerebral blood flow in Parkinson's disease with and without dementia. Neuroimage 2003;20:1309–19.

Cancer Investigation, 25:154–162, 2007
ISSN: 0735-7907 print / 1532-4192 online

DOI: 10.1080/07357900701208931

informa
healthcare

ORIGINAL ARTICLE

Expression of Glucose Transporter-1, Hexokinase-II, Proliferating Cell Nuclear Antigen and Survival of Patients with Pancreatic Cancer

Andrej Lyshchik, M.D., Ph.D.,[1] Tatsuya Higashi, M.D., Ph.D.,[1] Tadashi Hara, M.D.,[1] Yuji Nakamoto, M.D., Ph.D.,[1] Koji Fujimoto, M.D., Ph.D.,[2] Ryuichiro Doi, M.D., Ph.D.,[2] Masayuki Imamura, M.D., Ph.D.,[1] Tsuneo Saga, M.D., Ph.D.,[1] and Kaori Togashi, M.D., Ph.D.[1]

Department of Diagnostic Imaging and Nuclear Medicine, Kyoto University Graduate School of Medicine, Kyoto, Japan.[1]
Department of Surgery and Surgical Basic Science, Kyoto University Graduate School of Medicine, Kyoto, Japan.[2]

ABSTRACT

Objectives: **18F-fluoro-2-deoxy-D-glucose (FDG) positron emission tomography (PET) has been shown to be useful in diagnosis and staging of pancreatic cancer. However, the prognostic value of FDG-PET remains controversial. The aim of this study was to evaluate relations between the factors suggested to be related to the FDG accumulation in tumor tissue, such as glucose transporter-1 (GLUT-1), hexokinase type-II (HK-II), proliferating cell nuclear antigen (PCNA), and survival of pancreatic cancer patients.** ***Methods***: **Histological specimen of pancreatic cancer obtained from seventy-four consecutive patients were evaluated for the expression of GLUT-1, HK-II, and PCNA by visual analysis of immunohistochemical staining of paraffin sections from the tumor specimens using anti-GLUT-1, anti-HK-II, and anti-PCNA antibody, respectively. The percentages of cells strongly expressing GLUT-1, HK-II and PCNA were scored on a 5-point scale (1 = 0–20 percent, 2 = 20–40 percent, 3 = 40–60 percent, 4 = 60–80 percent, 5 = 80–100 percent). After initial treatment, each patient was followed-up and survival time was recorded. Median survival curves of the patients with different levels of GLUT-1, HK-II, and PCNA expression were evaluated using the Kaplan-Meier method. Statistical significance of the differences in survival was calculated with the log rank test.** ***Results***: **Median survival of examined patients showed no relation with the levels of GLUT-1 expression, while patients with low expression of HK-II (HK-II index < 3) had significantly shorter survival than those with higher expression of HK-II (HK-II index ≥ 3) (6.5 ± 4.1 versus 12.9 ± 22.4 months, respectively, $p < 0.05$). Median survival of examined patients also showed significant relations with the levels of PCNA expression. Patients with low expression of PCNA (PCNA index < 4) had significantly longer survival than those with higher expression of PCNA (PCNA index ≥ 4) (11.9 ± 20.1 versus, 5.8 ± 10.8 months, respectively, $p < 0.01$):** ***Conclusions***: **Our results showed that the expression of GLUT-1 had no prognostic value in the examined patients with pancreatic cancer. On the other hand, high levels of HK-II expression and low levels of PCNA expression may allow accurate identification of the patient with longer survival who may benefit from intensive anticancer treatment.**

Keywords: Glucose transporter-1, Hexokinase-II, Proliferating cell nuclear antigen, Pancreatic cancer, Survival.
Correspondence to:
Andrej Lyshchik, M.D., Ph.D.
Department of Radiology and Radiological Sciences
Vanderbilt University Medical Center
CCC-1118 MCN, 1161 21st Av. South Nashville
TN 37232-2675, USA
email: andrej.lyschik@vanderbilt.edu

INTRODUCTION

Pancreatic cancer remains a highly lethal disease in spite of new developments in early diagnosis, improvements in surgical morbidity and mortality, and the introduction of promising adjuvant and neoadjuvant therapies (1). In the minority of patients who present with disease limited to the pancreas, peri-ampullary region and peripancreatic lymph nodes, surgical resection (pancreaticoduodenectomy or distal pancreatectomy)